

MIIND : A Model-Agnostic Simulator of Neural Populations

Hugh Osborne¹, Yi Ming Lai², Mikkel Elle Lepperød³, David Sichau⁴, Lukas Deutz¹ and Marc de Kamps^{1,*}

¹ Institute for Artificial Intelligence and Biological Computation, School of Computing, University of Leeds, Leeds, United Kingdom

² School of Medicine, University of Nottingham, Nottingham, United Kingdom

³ Centre for Integrative Neuroplasticity, University of Oslo, Oslo, Norway

⁴ Department of Computer Science, ETH Zurich, Zurich, Switzerland

Correspondence*:

Marc de Kamps

M.deKamps@leeds.ac.uk

2 ABSTRACT

3 MIIND is a software platform for easily and efficiently simulating the behaviour of interacting
4 populations of point neurons governed by any 1D or 2D dynamical system. The simulator is
5 entirely agnostic to the underlying neuron model of each population and provides an intuitive
6 method for controlling the amount of noise which can significantly affect the overall behaviour. A
7 network of populations can be set up quickly and easily using MIIND's XML-style simulation file
8 format describing simulation parameters such as how populations interact, transmission delays,
9 post-synaptic potentials, and what output to record. During simulation, a visual display of each
10 population's state is provided for immediate feedback of the behaviour and population activity
11 can be output to a file or passed to a Python script for further processing. The Python support
12 also means that MIIND can be integrated into other software such as The Virtual Brain. MIIND's
13 population density technique is a geometric and visual method for describing the activity of each
14 neuron population which encourages a deep consideration of the dynamics of the neuron model
15 and provides insight into how the behaviour of each population is affected by the behaviour of its
16 neighbours in the network. For 1D neuron models, MIIND performs far better than direct simulation
17 solutions for large populations. For 2D models, performance comparison is more nuanced but the
18 population density approach still confers certain advantages over direct simulation. MIIND can be
19 used to build neural systems that bridge the scales between an individual neuron model and a
20 population network. This allows researchers to maintain a plausible path back from mesoscopic to
21 microscopic scales while minimising the complexity of managing large numbers of interconnected
22 neurons. In this paper, we introduce the MIIND system, its usage, and provide implementation
23 details where appropriate.

24 **Keywords:** Simulator, Neural Population, Population Density, Software, Python, Dynamical Systems, Network, GPU

1 INTRODUCTION

25 1.1 Population-Level Modeling

26 Structures in the brain at various scales can be approximated by simple neural population networks
27 based on commonly observed neural connections. There are a great number of techniques to simulate the
28 behaviour of neural populations with varying degrees of granularity and computational efficiency. At the
29 highest detail, individual neurons can be modelled with multiple compartments, transport mechanisms, and
30 other biophysical attributes. Simulators such as GENESIS (Wilson et al., 1988; Bower and Beeman, 2012)
31 and NEURON (Hines and Carnevale, 2001) have been used for investigations of the cerebellar microcircuit
32 (D’Angelo et al., 2016) and a thalamocortical network model (Traub et al., 2005). Techniques which
33 simulate the individual behaviour of point neurons such as in NEST (Gewaltig and Diesmann, 2007), or
34 the neuromorphic system SpiNNaker (Furber et al., 2014), allow neurons to be individually parameterised
35 and connections to be heterogeneous. This is particularly useful for analysing information transfer such as
36 edge detection in the visual cortex. They can also be used to analyse so called finite-size effects where
37 population behaviour only occurs as a result of a specific realisation of individual neuron behaviour. There
38 are, however, performance limitations on very large populations in terms of both computation speed and
39 memory requirements for storing the spike history of each neuron.
40

41 At a less granular level, rate-based techniques are a widely used practice of modeling neural activity with
42 a single variable, whose evolution is often described by first-order ordinary differential equations, which
43 goes back to Wilson and Cowan (1972). The Virtual Brain (TVB) uses these types of models to represent
44 activity of large regions (nodes) in whole brain networks to generate efficient simulations (Sanz Leon et al.,
45 2013; Jirsa et al., 2014). TVB demonstrates the benefits of a rate based approach with the Epileptor neural
46 population model yielding impressive clinical results (Proix et al., 2017). The Epileptor model is based
47 on the well known Hindmarsh-Rose neuron model (Hindmarsh and Rose, 1984). However, the behaviour
48 of this and other rate based models is defined at the population level instead of behaviour emerging from
49 a definition of the underlying neurons. Therefore, these models have less power to explain simulated
50 behaviours at the microscopic level.
51

52 Between these two extremes of granularity is a research area which bridges the scales by deriving
53 population level behaviour from the behaviour of the underlying neurons. So called population density
54 techniques (PDTs) have been used for many years (Knight, 1972; Knight et al., 1996; Omurtag et al., 2000)
55 to describe a population of neurons in terms of a probability density function. The transfer function of a
56 neuron model or even an experimental neural recording can be used to approximate the response from a
57 population using this technique (Wilson and Cowan, 1972; El Boustani and Destexhe, 2009; Carlu et al.,
58 2020). However, analytical solutions are often limited to regular spiking behaviour with constant or slowly
59 changing input. The software we present here, MIIND, provides a numerical solution for populations of
60 neurons with potentially complex behaviours (for example bursting) receiving rapidly changing noisy input
61 with arbitrary jump sizes. The noise is usually assumed to be shot noise, but can be non-Markovian (Lai and
62 de Kamps, 2017). It contains a number of features that make it particularly suitable for dynamical systems
63 representing neuronal dynamics, such as an adequate handling of boundary conditions that emerge from the
64 presence of thresholds and reset mechanisms, but is not restricted to neural systems. The dynamical systems
65 can be grouped in large networks, which can be seen as the model of a neural circuit at the population level.
66

67 The key idea behind MIIND is shown in Fig. 1A. Here, a population of neurons is simulated. In this case,
68 the neurons are defined by a conductance based leaky-integrate-and-fire neuron model with membrane
69 potential and state of the conductance as the two variables. The neuron's evolution through state space is
70 given by a two-dimensional dynamical system. The positions of individual neurons change in state space,
71 both under the influence of the neuron's endogenous dynamics as determined by the dynamical system and
72 of spike trains arriving from neurons in other populations, which cause rapid transitions in state space that
73 are modeled as instantaneous jumps. For the simulation techniques mentioned earlier involving a large
74 number of individual model neuron instances, a practice that we will refer to as Monte Carlo simulation,
75 the population can be represented as a cloud of points in state space. The approach in MIIND, known as
76 a population density technique (PDT) models the probability density of the cloud, shown in Fig. 1 as a
77 heat map, rather than the behaviour of individual neurons. The threshold and reset values of the underlying
78 neuron model are visible in the hard vertical edges of the density in Fig. 1A. In Fig. 1B, the same simulation
79 approach is used for a population of Fitzhugh-Nagumo neurons (FitzHugh, 1961; Nagumo et al., 1962).
80 The Fitzhugh-Nagumo model has no threshold-reset mechanism and so there are no vertical boundaries to
81 the density. As well as being informative in themselves, common population metrics such as average firing
82 rate and **The Case for Population Density Techniques** are calculated from these density functions.

83 Why use this technique? Omurtag et al. (2000); Nykamp and Tranchina (2000); Kamps (2003); Iyer
84 et al. (2013) have demonstrated that PDTs are much faster than Monte Carlo simulation for 1D models;
85 De Kamps et al. (2019) have shown that while speed is comparable between 2D models and Monte Carlo,
86 memory usage is orders of magnitude lower because no spikes need to be buffered, which accounts for
87 significant memory use in large-scale simulations. In practice, this may make the difference between
88 running a simulation on an HPC cluster or a single PC equipped with a general purpose graphics processing
89 unit (GPU).

90 Apart from simulation speed, PDTs have been important in understanding population level behaviour
91 analytically. Important questions, such as 'why are cortical networks stable?' (Amit and Brunel, 1997),
92 'how can a population be oscillatory when its constituent neurons fire sporadically?' (Brunel and Hakim,
93 1999), 'how does spike shape influence the transmission spectrum of a population?' (Fourcaud-Trocmé
94 et al., 2003) have been analysed in the context of population density techniques, providing insights that
95 cannot be obtained from merely running simulations. A particularly important question, which has not been
96 answered in full is: 'how do rate-based equations emerge from populations of spiking neurons and when is
97 their use appropriate?'. There are many situations where such rate-based equations are appropriate, but
98 some where they are not and their correspondence to the underlying spiking neural dynamics is not always
99 clear (Montbrió et al., 2015; de Kamps, 2013). There is a body of work suggesting that some rate-based
100 equations can be seen as the lowest order of perturbations of a stationary state, and much of this work is
101 PDT-based (Wilson and Cowan, 1972; Gerstner, 1998; Mattia and Del Giudice, 2002, 2004; Montbrió
102 et al., 2015). MIIND opens the possibility to incorporate these theoretical insights into large-scale network
103 models. For example, we can demonstrate the prediction from Brunel and Hakim (1999) that inhibitory
104 feedback on a population can cause a bifurcation and produce resonance. Finally, for a steady state input,
105 the firing rate prediction of a PDT model converges to a transfer function which can be used in artificial
106 spiking neural networks.
107

110 1.3 Population-level Modeling

111 For the population density approach we take with MIIND, the time evolution of the probability density
 112 function is described by a partial integro-differential equation. We give it here to highlight some of its
 113 features, but for an in depth introduction to the formalism and a derivation of the central equations we refer
 114 to Omurtag et al. (2000).

$$\frac{\partial \rho}{\partial t} + \frac{\partial}{\partial \vec{v}} \cdot \left(\frac{\vec{F}(\vec{v})\rho(\vec{v}, t)}{\tau} \right) = \int_M d\vec{v}' \left\{ W(\vec{v} \mid \vec{v}')\rho(\vec{v}') - W(\vec{v}' \mid \vec{v})\rho(\vec{v}) \right\}, \quad (1)$$

115 ρ is the probability density function defined over a volume of state space, M , in terms of time, t , and
 116 time-dependent variables, \vec{v} , under the assumption that the neuronal dynamics of a point model neuron is
 117 given by:

$$\tau \frac{d\vec{v}}{dt} = \vec{F}(\vec{v}), \quad (2)$$

118 where τ is the neuron's membrane time constant. Simple models are one-dimensional (1D). For the
 119 leaky-integrate-and-fire (LIF) neuron:

$$F(v) = -v, \quad (3)$$

120 For a quadratic-integrate-and-fire (QIF) neuron:

$$F(v) = v^2 + I, \quad (4)$$

121 where v is the membrane potential, and I can be interpreted as a bifurcation parameter. More complex
 122 models require a higher dimensional state space. Since such a space is hard to visualise and understand,
 123 considerable effort has been invested in the creation of effective models. In particular two-dimensional
 124 (2D) models are considered to be a compromise that allows considerably more biological realism than LIF
 125 or QIF neurons, but which remain amenable to visualisation and analysis, and can often be interpreted
 126 geometrically (Izhikevich, 2007). Examples are the Izhikevich simple neuron (Izhikevich, 2003), the
 127 Fitzhugh-Nagumo neuron (FitzHugh, 1961; Nagumo et al., 1962), and the adaptive-exponential-integrate-
 128 and-fire neuron (Brette and Gerstner, 2005), incorporating phenomena such as bursting, bifurcations,
 129 adaptation, and others that cannot be accounted for in a one dimensional model.

130 $W(v \mid v')$ in Eq. 1 represents a transition probability rate function. The right hand side of Eq. 1 makes it
 131 a Master equation. Any Markovian process can be represented by a suitable choice of W . For example, for
 132 shot noise, we have

$$W(v' \mid v) = \nu(\delta(v' - v - h) - \delta(v - v')), \quad (5)$$

133 where ν is the rate of the Poisson process generating spike events. The delta functions reflect that an
 134 incoming spike causes a rapid change in state space, modeled as an instantaneous jump, h . It depends on the
 135 particular neural model in what variable the jumps take place. Often models use a so-called delta synapse,
 136 such that the jump is in membrane potential. In conductance based models, the incoming spike causes a
 137 jump in the conductance variable (Fig. 1A), and the influence of the incoming spike on the potential is then
 138 indirect, given by the dynamical system's response to the sudden change in the conductance state.

139 MIIND produces a numerical solution to Eq. 1 for arbitrary 1D or 2D versions of $\vec{F}(\vec{v})$ (support for 3D
 140 versions is in development), under a broad variety of noise processes. Indeed, the right hand side of Eq. 1

141 can be generalised to non-Markov processes which cannot simply be formulated in terms of a transition
 142 probability rate function W . It is possible to introduce a right hand side that entails an integration over a
 143 past history of the density using a kernel whose shape is determined by a non-Markov process (Lai and
 144 de Kamps, 2017).

145

146 1.4 Quick Start Guide

147 Before describing the implementation details of MIIND, this section demonstrates how to quickly
 148 set up a simulation for a simple E-I network of populations of conductance based neurons using the
 149 MIIND Python library. A rudimentary level of Python experience is needed to run the simulation. In
 150 most cases, MIIND can be installed via Python pip. Detailed installation instructions can be found in
 151 the *README.md* file of the MIIND repository (De Kamps et al., 2020). For this example, we will use a
 152 pre-written script, *generateCondFiles.py*, to generate the required simulation files which can be found in
 153 the *examples/quick_start* directory of the MIIND repository or can be loaded into a working directory using
 154 the following python command.

155 \$ python -m miind.loadExamples

156 In the *examples/quick_start* directory, the *generateCondFiles.py* script generates the simulation files,
 157 *cond.model* and *cond.tmat*.

158 \$ python generateCondFiles.py

159 The contents of *generateCondFiles.py* is given in Listing 1. The two important parts of the script
 160 are the neuron model function, in this case named *cond()*, and the call to the MIIND function
 161 *grid_generate.generate()* which takes a number of parameters which are discussed in detail later.

Listing 1. *generateCondFiles.py*

```
162 import miind.grid_generate as grid_generate
163
164 def cond(y,t):
165     E_r = -65e-3
166     tau_m = 20e-3
167     tau_s = 5e-3
168
169     v = y[0];
170     h = y[1];
171
172     v_prime = ( -(v - E_r) - (h * v) ) / tau_m
173     h_prime = -h / tau_s
174
175     return [v_prime, h_prime]
176
177 grid_generate.generate(
178     func = cond,
179     timestep = 1e-04,
180     timescale = 1,
181     tolerance = 1e-6,
182     basename = 'cond',
183     threshold_v = -55.0e-3,
184     reset_v = -65e-3,
185     reset_shift_h = 0.0,
186     grid_v_min = -72.0e-3,
```

```

187     grid_v_max = -54.0e-3,
188     grid_h_min = -1.0,
189     grid_h_max = 2.0,
190     grid_v_res = 200,
191     grid_h_res = 200,
192     efficacy_orientation = 'h')

```

193 The *cond()* function should be familiar to those who have used Python numerical integration frameworks
 194 such as *scipy.integrate*. It takes the two time dependent variables defined by $y[0]$ and $y[1]$ and a placeholder
 195 parameter, t , for performing a numerical integration. In the function, the user may define how the derivatives
 196 of each variable are to be calculated. The *generate()* function requires a suitable time step, values for a
 197 threshold and reset if needed, and a description of the extent of the state space to be simulated. With this
 198 structure, the user may define any two dimensional neuron model. The generated files are then referenced
 199 in a second file which describes a network of populations to be simulated. Listing 2 shows the contents of
 200 *cond.xml* describing an E-I network which uses the generated files from *generateCondFiles.py*.

Listing 2. *cond.xml*

```

201 <Simulation>
202   <WeightType>CustomConnectionParameters</WeightType>
203   <Algorithms>
204     <Algorithm type="GridAlgorithm" name="COND" modelfile="cond.model" tau_refractive="0.0"
205       ↪ transformfile="cond_0_0_0_0_.tmat" start_v="-0.065" start_w="0.0" >
206       <TimeStep>1e-04</TimeStep>
207     </Algorithm>
208     <Algorithm type="RateFunctor" name="ExcitatoryInput">
209       <expression>800.</expression>
210     </Algorithm>
211   </Algorithms>
212   <Nodes>
213     <Node algorithm="ExcitatoryInput" name="INPUT_E" type="EXCITATORY_DIRECT" />
214     <Node algorithm="ExcitatoryInput" name="INPUT_I" type="EXCITATORY_DIRECT" />
215     <Node algorithm="COND" name="E" type="EXCITATORY_DIRECT" />
216     <Node algorithm="COND" name="I" type="INHIBITORY_DIRECT" />
217   </Nodes>
218   <Connections>
219     <Connection In="INPUT_E" Out="E" num_connections="1" efficacy="0.1" delay="0.0"/>
220     <Connection In="INPUT_I" Out="I" num_connections="1" efficacy="0.1" delay="0.0"/>
221     <Connection In="E" Out="I" num_connections="1" efficacy="0.1" delay="0.001"/>
222     <Connection In="E" Out="E" num_connections="1" efficacy="0.1" delay="0.001"/>
223     <Connection In="I" Out="E" num_connections="1" efficacy="-0.1" delay="0.001"/>
224     <Connection In="I" Out="I" num_connections="1" efficacy="-0.1" delay="0.001"/>
225   </Connections>
226   <Reporting>
227     <Display node="E" />
228     <Display node="I" />
229     <Rate node="E" t_interval="0.001" />
230     <Rate node="I" t_interval="0.001" />
231   </Reporting>
232   <SimulationRunParameter>
233     <SimulationName>EINetwork</SimulationName>
234     <t_end>0.2</t_end>
235     <t_step>1e-04</t_step>
236     <name_log>einetwork.log</name_log>

```

```
237     </SimulationRunParameter>
238 </Simulation>
```

239 The full syntax documentation for MIIND XML files is given in section 4. Though more compact or
 240 flexible formats are available, XML was chosen as a formatting style due to its ubiquity ensuring the
 241 majority of users will already be familiar with the syntax. The *Algorithms* section is used to declare specific
 242 simulation methods for one or more populations in the network. In this case, a GridAlgorithm named
 243 *COND* is set up which references the *cond.model* and *cond.tmat* files. A RateFunctor algorithm produces a
 244 constant firing rate. In the *Nodes* section, two instances of *COND* are created: one for the excitatory and
 245 inhibitory populations respectively. Two *ExcitatoryInput* nodes are also defined. The *Connections* section
 246 allows us to connect the input nodes to the two conductance populations. The populations are connected to
 247 each other and to themselves with a 1ms transmission delay. The remaining sections are used to define how
 248 the output of the simulation is to be recorded, and to provide important simulation parameters such as the
 249 simulation time. By running the following python command, the simulation can be run.

Listing 3. Run the cond.xml simulation.

```
250 $ python -m miind.run cond.xml
```

251 The probability density plots for both populations will be displayed in separate windows as the simulation
 252 progresses. The firing rate of the excitatory population can be plotted using the following commands. Fig.
 253 2 shows the probability density plots for both populations and average firing rate of population E.

Listing 4. Load the cond.xml simulation and plot the average firing rate of population E.

```
254 $ python -m miind.miindio sim cond.xml
255 $ python -m miind.miindio rate E
```

256 Finally, the density function of each population can be plotted as a heat map for a given time in the
 257 simulation.

Listing 5. Plot the probability density of population I at time 0.12s.

```
258 $ python -m miind.miindio plot-density I 0.12
```

259 Later sections will show how the MIIND simulation can be imported into a user defined Python script
 260 so that input can be dynamically set during simulation and population activity can be captured for further
 261 processing.

2 THE MIIND GRID ALGORITHM

262 MIIND allows the user to simulate populations of any 1D or 2D neuron model. Although much of MIIND's
 263 architecture is agnostic to the integration technique used to simulate each population, the system is primarily
 264 designed to make use of its novel population density techniques, grid algorithm and mesh algorithm. Both
 265 algorithms use a discretisation of the underlying neuron model's state space such that each discrete "cell",
 266 which covers a small area of state space, is considered to hold a uniform distribution of probability mass.
 267 In both algorithms, MIIND performs three important steps for each iteration. First, probability mass is
 268 transferred from each cell to one or more other cells according to the dynamics of the underlying neuron
 269 model in the absence of any input. The probability mass is then spread across multiple other cells due to
 270 incoming random spikes. Finally, if the underlying neuron model has a threshold-reset mechanic, such as
 271 an integrate and fire model, probability mass which has passed the threshold is transferred to cells along
 272 the reset potential. As it is the most practically convenient method for the user, we will first introduce the

273 grid algorithm. We will discuss its benefits and weaknesses, indicating where it may be appropriate to use
 274 the mesh algorithm instead.

275

276 2.1 Generating the Grid and Transition Matrix

277 To discretise the state space in the grid method, the user can specify the size and $M \times N$ resolution of
 278 a rectangular grid which results in MN identical rectangular cells, each of which will hold probability
 279 mass. In the grid algorithm, a transition matrix lists the proportion of mass which moves from each cell to
 280 (usually) adjacent cells in one time step due to the deterministic dynamics of the underlying neural model.
 281 To pre-calculate the transitions for each cell, MIIND first translates the vertices of every cell by integrating
 282 each point forward by one time step according to the dynamics of the underlying neuron model as shown
 283 in Fig. 3A. As the time step is small, a single Euler step is usually all that is required to avoid large errors
 284 (although other integration schemes can be used if required). Each transformed cell is no longer guaranteed
 285 to be a rectangle and is compared to the original non-transformed grid to ascertain which cells overlap with
 286 the newly generated quadrilateral. An overlap indicates that some proportion of neurons in the original
 287 cell will move to the overlapping cell after one time step. In order to calculate the overlap, the algorithm
 288 in Listing 6 is employed. This algorithm is also used in the geometric method of generating transition
 289 matrices for the mesh algorithm shown later.

Listing 6. A pseudo-code representation of the algorithm used to calculate the overlapping areas between transformed grid cells and the original grid (or for translated cells of a mesh). The proportion of the area of the original cell gives the proportion of probability mass to be moved in each transition.

290 For each transformed cell, A, in the grid:
 291 Translate all four vertices according to a single Euler step.
 292 Split A into two triangles and add them to a triangle list.
 293 For each non-transformed cell, B:
 294 Set the overlapping area sum to 0.
 295 While the triangle list has changed:
 296 For each triangle in the list:
 297 If the triangle is entirely outside B: add 0 to the sum.
 298 If the triangle is entirely within B: add the triangle's area to the sum.
 299 If B is entirely within the triangle: add B's area to the sum.
 300 Else: For each edge in B:
 301 Calculate any intersection points with the edges of the triangle.
 302 Triangulate the polygon produced by the original triangle points plus the new intersection
 303 → points.
 304 Remove the original triangle from the list.
 305 Add the newly generated triangles to the list.
 306 Calculate the proportion of A taken by the sum.
 307 Add the transition from A to B with the proportion to the transition matrix.

308 Though the pseudo-code algorithm is order N^2 , there are many ways that the efficiency of the algorithm
 309 is improved in the implementation. The number of non-transformed cells checked for overlap can be limited
 310 to only those which lie underneath each given triangle. Furthermore, the outer loop is parallelisable. Finally,
 311 as the non-transformed cells are axis-aligned rectangles, the calculation to find edge intersections is trivial.
 312 Fig. 3A shows a fully translated and triangulated cell at the end of the algorithm. Once the transition matrix
 313 has been generated, it is stored in a file with the extension *.tmat*. Although the regular grid can be described
 314 with only four parameters (the width, height, X, and Y resolutions), to more closely match the behaviour of
 315 mesh algorithm, the vertices of the grid are stored in a *.model* file. To simulate a population using the grid

316 algorithm, the *.tmat* and *.model* files must be generated and referenced in the XML simulation file.

317

318 As demonstrated in the quick start guide (section 1.4), to generate a *.model* and *.tmat* file, the user must
319 write a short Python script which defines the underlying neuron model and makes a call to the MIIND API
320 to run the algorithm in listing 6. In the *python* directory of the MIIND source repository (see section 1
321 in the supplementary material), there are a number of examples of these short scripts. The script used to
322 generate a grid for the Izhikevich simple model is listed in the supplementary material section 9.1. The
323 required definition of the neuron model function is similar to those used by many numerical integration
324 libraries. The function takes a parameter, *y*, which represents a list which holds the two time dependent
325 variables and a parameter, *t*, which is a placeholder for use in integration. The function must return the first
326 time derivatives of each variable as a list in the same order as in *y*. Once the function has been written, a
327 call to *grid_generate.generate* is made which takes the parameters listed in Table 1.

328 When the user runs the script, the required *.model* and *.tmat* files will be generated for use in a simulation.
329 In the quick start guide, the conductance based neuron model requires that *efficacy_orientation* is set to
330 ‘h’ because incoming spikes cause an instantaneous change in the conductance variable instead of the
331 membrane potential. By default, however, this parameter is set to ‘v’. When choosing values for the grid
332 bounds (*grid_v_min*, *grid_v_max*, *grid_h_min*, and *grid_h_max*), the aim is to estimate where in state space
333 the population density function might be non-zero during a simulation. In the conductance based neuron
334 model, because of the threshold-reset mechanic, the *grid_v_max* parameter need only be slightly above
335 the threshold to ensure that there is at least one column of cells on or above threshold to allow probability
336 mass to be reset. The *grid_v_min* value should be below the resting potential and reset potential. However,
337 we must also consider that the neurons could receive inhibitory spikes which would cause the neurons to
338 hyperpolarise. *grid_v_min* should therefore be set to a value beyond the lowest membrane potential expected
339 during the simulation. Similarly for the conductance variable, space should be provided for reasonable
340 positive and negative values. If it is known beforehand that no inhibition will occur, however, then the state
341 space bounds can be set tighter in order to improve the accuracy of the simulation using the same grid
342 resolution (*grid_v_res* and *grid_h_res*). If, during the simulation, probability mass is pushed beyond the
343 lower bounds of the grid, it will be pinned at those lower bounds which will produce incorrect behaviour
344 and results. If the probability mass is pushed beyond the upper bounds, it will be wrapped around to the
345 lower bounds which will also produce incorrect results. The choice of grid resolution is a balance between
346 speed of simulation and accuracy. However, even very coarse grids can produce representative firing rates
347 and behaviours. Typical grid resolutions range between 100x100 and 500x500. It can also be beneficial
348 to experiment with different *M* and *N* values as the accuracy of each dimension can have unbalanced
349 influence over the population level metrics.

350 351 2.2 The Effect of Random Incoming Spikes

352 The transition matrix in the *.tmat* file describes how probability mass moves to other cells due to the
353 deterministic dynamics of the underlying neuron model. The transition matrix is sparse as probability mass
354 is often only transferred to nearby cells. Solving the deterministic dynamics is therefore very efficient. The
355 mesh algorithm is even faster and, as demonstrated later, is significantly quicker than direct simulation
356 for this part of the algorithm. Another benefit to the modeler is that by rendering the grid with each cell
357 coloured according to its mass, the resultant heat map gives an excellent visualisation of the state of the
358 population as a whole at each time step of the simulation as shown in Fig. 2. This provides particularly

359 useful insight into the sub-threshold behaviour of neurons in the population.
 360

361 The second step of the grid algorithm, which must be performed every iteration, is to solve the change
 362 in the probability density function due to random incoming spikes. It is assumed that a spike causes an
 363 instantaneous change in the state of a neuron, usually a step wise jump in membrane potential corresponding
 364 to a constant synaptic efficacy. In the conductance based neuron example, this jump is in the conductance.
 365 When considering each cell in the grid, a single incoming spike will cause some proportion of the
 366 probability mass to shift to at most, two other cells as shown in Fig. 3. Because all cells in the grid are
 367 equally distributed and the same size, the relative transition of probability mass caused by a single spike is
 368 the same for them all. A sparse transition matrix, M , can be generated from this single transition so that
 369 applying M to the probability density grid applies the transition to all cells. MIIND calculates a different
 370 M for each incoming connection to the population based on the user defined instantaneous jump, which
 371 we refer to as the efficacy. In the mesh algorithm, the relative transitions are different for each cell and so a
 372 transition matrix (similar to that of the *.tmat* file) is required to describe the effect of a single spike. As with
 373 many other population density techniques, MIIND assumes that incoming spikes are Poisson distributed,
 374 although it is possible to approximate other distributions. MIIND uses M to calculate the change to the
 375 probability density function, ρ , due solely to the non-deterministic dynamics as described by equation 6.

$$d\rho/dt = \lambda M \rho \quad (6)$$

376 λ is the incoming Poisson firing rate. The boost numeric library is used to integrate $d\rho/dt$. The solution
 377 to this equation describes the spread of the probability density due to Poisson spikes. This ‘master process’
 378 step amounts to multiple applications of the transition matrix M and is where the majority of time is taken
 379 computationally. However, OpenMP is available in MIIND to parallelise the matrix multiplication. If
 380 multiple cores are available, the OpenMP implementation significantly improves performance of the master
 381 process step. More information covering this technique can be found in De Kamps et al. (2019); de Kamps
 382 (2013).

383 2.3 Threshold-Reset Dynamics

384 Many neuron models include a “threshold-reset” process such that neurons which pass a certain mem-
 385 brane potential value are shifted back to a defined reset potential to approximate repolarisation during an
 386 action potential. To facilitate this in MIIND, after each iteration, probability mass in cells which lie across
 387 the threshold potential is relocated to cells which lie across the reset potential according to a pre-calculated
 388 mapping. Often, a refractory period is used to hold neurons at the reset potential before allowing them to
 389 again receive incoming spikes. In MIIND this is implemented using a queue for each threshold cell as
 390 shown in Fig. 4. The queues are set to the length of the refractory period divided by the time step, rounded
 391 up to the nearest integer value. During each iteration, probability mass is shifted one position along the
 392 queue. A linear interpolation of the final two places in the queue is made and this value is passed to the
 393 mapped reset cell. The interpolation is required in case the refractory period is not an integer multiple of
 394 the time step. The total probability mass in the threshold cells each iteration is used to calculate the average
 395 population firing rate. For models which do not require threshold-reset dynamics, setting the threshold
 396 value to the maximal membrane potential of the grid, and the reset to the minimal membrane potential
 397 ensures that no resetting of probability mass will occur.
 398

400 2.4 How MIIND Facilitates Interacting Populations

401 The grid algorithm describes how the behaviour of a single population is simulated. The MIIND software
402 platform as a whole provides a way for many populations with possibly many different integration algo-
403 rithms to interact in a network. The basic process of simulating a network is as follows. The user must
404 write an XML file which describes the whole simulation. This includes defining the population nodes of
405 the network and how they are connected; which integration technique each population uses (grid algorithm,
406 mesh algorithm etc.); external inputs to the network; how the activity of each population will be recorded
407 and displayed; the length and time step of the simulation. As shown in the quick start guide, the XML file
408 can be passed as a parameter to the *miind.run* module in Python. When the simulation is run, a population
409 network is instantiated and the simulation loop is started. For each iteration, the output activity of each
410 population node is recorded. By default, the activity is assumed to be an average firing rate but other options
411 are available such as average membrane potential. The outputs are passed as inputs to each population node
412 according to the connectivity defined in the XML file. Each population is evolved forward by one time
413 step and the simulation loop repeats until the simulation time is up. The Python front end, *miind.miindio*,
414 provides the user with tools to analyse the output from the simulation. A custom *run* script can also be
415 written by the user to perform further analysis and processing.
416

417 The simplicity of the XML file means that a user can set up a large network of populations with very
418 little effort. The model archive in the code repository holds a set of example simulations demonstrating the
419 range of MIIND’s functionality and includes an example which simulates the Potjans-Diesmann model
420 of a cortical microcircuit (Potjans and Diesmann, 2014), which is made up of eight populations of leaky
421 integrate and fire neurons. Fig. 5 shows a representation of the model with embedded density plots for each
422 population.
423

424 2.5 Running MIIND Simulations

425 The quick start guide demonstrated the simplest way to run a simulation given that the required *.model*,
426 *.tmat*, and *.XML* files have been generated. The *miind.run* script imports the *miind.miindsim* Python
427 extension module which can also be imported into any user written Python script. Section 6 details the
428 functions which are exposed by *miind.miindsim* for use in a python script. The benefit of this method is
429 that the outputs from populations can be recorded after each iteration and inputs can be dynamic allowing
430 the python script to perform its own logic on the simulation based on the current state.
431 There is also a command line interface (CLI) program provided by the Python module, *miind.miindio*. The
432 CLI can be used for many simple work flow tasks such as generating models and displaying results. Each
433 command which is available in the CLI, can also be called from the MIIND Python API, upon which the
434 CLI is built. A full list of the available commands in the CLI is given in section 9.3 of the supplementary
435 material and a worked example using common CLI commands is provided in section 7.
436

437 2.6 When not to use the Grid Algorithm

438 For many underlying neuron models, the grid algorithm will produce results showing good agreement
439 with direct simulation to a greater or lesser extent depending on the resolution of the grid (see Fig. 6).
440 However, for models such as exponential integrate and fire, a significantly higher grid resolution is required
441 than might be expected because of the speed of the dynamics across the threshold (beyond which, neurons
442 perform the action potential). When the input rate is high enough to generate tonic spiking in an exponential
443 integrate and fire model, the rate of depolarisation of each neuron reduces as it approaches the threshold

444 potential then once it is beyond the threshold, quickly increases producing a spike. Because the grid
445 discretises the state space into regular cells, if cells are large due to a low resolution, only a small number
446 of cells will span the threshold, as shown in Fig. 7A. When the transition matrix is applied each time
447 step, probability mass is distributed uniformly across each cell. Probability mass can therefore artificially
448 cross the threshold much faster than it should leading to a higher than expected average firing rate for the
449 population. Using the grid algorithm for such models where the firing rate itself is dependent on sharp
450 changes in the speed of the dynamics should be avoided if high accuracy is required. Other neuron models,
451 like the bursting Izhikevich simple model, also have sharp changes in speed when neurons transition from
452 bursting to quiescent periods. However, the bursting firing rate is unaffected by these dynamics and the
453 oscillation frequency is affected only negligibly due to the difference in timescales. The grid algorithm
454 is therefore still appropriate in cases such as this. For exponential integrate and fire models, however,
455 MIIND provides a second algorithm which can more accurately capture the deterministic dynamics: mesh
456 algorithm.

3 THE MIIND MESH ALGORITHM

457 Instead of a regular grid to discretise the state space of the underlying neuron model, the mesh algorithm
458 requires a two dimensional mesh which describes the dynamics of the neuron model itself in the absence
459 of incoming spikes. A mesh is constructed from strips which follow the trajectories of neurons in state
460 space (Fig. 8). The trajectories form so-called characteristic curves of the neuron model from which this
461 method is inspired (De Kamps et al., 2019; de Kamps, 2013).

462 These trajectories are computed as part of a one-time preprocessing step using an appropriate integration
463 technique and time step. Strips will often approach or recede from nullclines and stationary points and
464 their width may shrink or expand according to their proximity to such elements. Each strip is split into
465 cells. Each cell represents how far along the strip neurons will move in a single time step. As with the
466 width of the strips, cells will become more dense or more sparse as the dynamics slow down and speed up
467 respectively. The result of covering the state space with strips is a precomputed description of the model
468 dynamics such that the state of a neuron in one cell of the mesh is guaranteed to be in the next cell along
469 the strip after a single time step. Depending on the underlying neuron model, it can be difficult to get full
470 coverage without cells becoming too small or shear. However, once built, the deterministic dynamics have
471 effectively been “pre-solved” and baked into the mesh.
472

473 As with the grid algorithm, when the simulation is running, each cell is associated with a probability
474 mass value which represents the probability of finding a neuron from the population with a state in that
475 cell. When a probability density function (PDF) is defined across the mesh, computing the change to the
476 PDF due to the deterministic dynamics of the neurons is simply a matter of shifting each cell’s probability
477 mass value along its strip. In the C++ implementation, this requires no more than a pointer update and is
478 therefore quicker than the grid algorithm for solving the deterministic dynamics as no transition matrix is
479 applied to the cells.
480

481 Mesh algorithm does, however, still require a transition matrix to implement the effect of incoming spikes
482 on the PDF. This transition matrix describes how the state of neurons in each cell are translated in the event
483 of a single incoming spike. Unlike the grid algorithm, cells are unevenly distributed across the mesh and
484 are different sizes and shapes. What proportion of probability mass is transferred to which cells with a
485 single incoming spike is, therefore, different for all cells. During simulation, the total change in the PDF is

486 calculated by shifting probability mass one cell down each strip and using the transition matrix to solve the
487 master equation every time step. The combined effect can be seen in Fig. 9. The method of solving the
488 master equation is explained in detail in de Kamps (2013).

489

490 3.1 When not to use the Mesh Algorithm

491 Just as with the grid algorithm, certain neuron models are better suited to an alternative algorithm. In
492 the mesh algorithm, very little error is introduced for the deterministic dynamics. Probability mass flows
493 down each strip as it would without the discretisation and error is limited only to the size of the cells.
494 When the master equation is solved, however, probability mass can spread to parts of state space which
495 would see less or no mass. Fig. 7B demonstrates how in the mesh algorithm, as probability mass is pushed
496 horizontally, very shear cells can allow mass to be incorrectly transferred vertically as well. In the the
497 grid algorithm, error is introduced in the opposite way. Solving the master equation pushes probability
498 mass along horizontal rows of the grid and error is limited to the width of the row. The grid algorithm is
499 preferable over the mesh algorithm for populations of neurons with one fast variable and one slow variable
500 which can produce very shear cells in a mesh, e.g. in the Fitzhugh-Nagumo model (De Kamps et al., 2019).
501 In both algorithms, the error can be reduced by increasing the density of cells (by increasing the resolution
502 of the grid, or by reducing the timestep and strip width of the mesh). However, better efficiency is achieved
503 by using the appropriate algorithm.

504

505 3.2 Building a Mesh for the Mesh Algorithm

506 Before a simulation can be run for a population which uses the mesh algorithm, the pre-calculation steps
507 of generating a mesh and transition matrices must be performed. Fig. 10 shows the full pre-processing
508 pipeline for mesh algorithm. The mesh is a collection of strips made up of quadrilateral cells. As mentioned
509 earlier, probability mass moves along a strip from one cell to the next each time step which describes
510 the deterministic dynamics of the model. Defining the cells and strips of a 2D mesh is not generally a
511 fully automated process and the points of each quadrilateral must be defined by the mesh developer and
512 stored in a *.mesh* file. When creating the mesh, the aim is to cover as much of the state space as possible
513 without allowing cells to get too small or misshapen. An example of a full mesh generation script for
514 the Izhikevich simple neuron model (Izhikevich, 2003) is available in section 9.1 of the supplementary
515 material. MIIND provides *miind.miind_api.LifMeshGenerator*, *miind.miind_api.QifMeshGenerator*, and
516 *miind.miind_api.EifMeshGenerator* scripts to automatically build the 1D leaky integrate and fire, quadratic
517 integrate and fire, and exponential integrate and fire neuron meshes respectively. They can be called from
518 the CLI. The scripts generate the three output files which any mesh generator script must produce: a *.mesh*
519 file, a *.stat* file which defines extra cells in the mesh to hold probability mass that has settled at a stationary
520 point, and a *.rev* file which defines a “reversal mapping” indicating how probability mass is transferred
521 from strips in the mesh to the stationary cells. More information on *.mesh*, *.stat*, and *.rev* files is provided
522 in the supplementary material section 6.

523

524 Once the *.mesh*, *.stat*, and *.rev* files have been generated by the user or by one of the automated 1D
525 scripts, the Python command line interface, *miind.miindio*, provides commands to convert the three files
526 into a single *.model* file and generate transition matrices stored in *.mat* files. The model file is what will be
527 referenced and read by MIIND to load a mesh for a simulation. To generate this file, use the CLI command,
528 **generate-model**. The command parameters are shown in Table 2. All input files must have the same base
529 name, for example: *lif.mesh*, *lif.stat*, and *lif.rev*. If the command runs successfully, a new file will be created:

530 *basename.model*. A number of pre-generated models are available in the *examples* directory of the MIIND
531 repository to be used “out of the box” including the adaptive exponential integrate and fire and conductance
532 based neuron models.

Listing 7. Generate a Model in the CLI

533 > generate-model lif -60.0 -30.0

534 The generated *.model* file contains the mesh vertices, some summary information such as the time step
535 used to generate the mesh and the threshold and reset values, and a mapping of threshold cells to reset cells.
536

537 In the the mesh algorithm, transition matrices are used to solve the Poisson master equation which
538 describes the movement of probability mass due to incoming random spikes. In the mesh algorithm, one
539 transition matrix is required for each post synaptic efficacy that will be needed in the simulation. So if a
540 population is going to receive spikes which cause jumps of 0.1mV and 0.5mV, two transition matrices are
541 required. It is demonstrated later how the efficacy can be made dependent on the membrane potential or
542 other variables. Each transition matrix is stored in a *.mat* file and contains a list of source cells, target cells,
543 and proportions of probability mass to be transferred to each. For a given cell in the mesh, neurons with a
544 state inside that cell which receive a single external spike will shift their location in state space by the value
545 of the efficacy. Neurons from the same cell could therefore end up in many other different cells, though
546 often ones which are nearby. It is assumed that neurons are distributed uniformly across the source cell.
547 Therefore, the proportion of neurons which end up in each of the other cells can be calculated. MIIND
548 performs this calculation in two ways, the choice for which is given to the user.
549

550 The first method is to use a Monte Carlo approach such that a number of points are randomly placed in
551 the source cell then translated according to the efficacy. A search takes place to find which cells the points
552 were translated to and the proportions are calculated from the number of points in each. For many meshes,
553 a surprisingly small number of points, around 10, is required in each cell to get a good approximation
554 for the transition matrix and the process is therefore quite efficient. As shown in Fig. 10, an additional
555 process is required when generating transition matrices using Monte Carlo which includes two further
556 intermediate files, *.fid* and *.lost*. All points must be accounted for when performing the search and in cases
557 where points are translated outside of the mesh, an exhaustive search must be made to find the closest cell.
558 The **lost** command allows the user to speed up this process which is covered in detail in section 6.1 of the
559 supplementary material.
560

561 The second method translates the actual vertices of each cell according to the efficacy and calculates the
562 exact overlapping area with other cells. The method by which this is achieved is the same as that used to
563 generate the transition matrix of the grid algorithm, described in section 2.1. This method provides much
564 higher accuracy than Monte Carlo but is one order of magnitude slower (it takes a similar amount of time
565 to perform Monte Carlo with 100 points per cell). For some meshes, it is crucial to include very small
566 transitions between cells to properly capture the dynamics which justifies the need for the slower method.
567 It also benefits from requiring no additional user input in contrast to the Monte Carlo method.
568

569 In *miind.miindio*, the command **generate-matrix** can be used to automatically generate each *.mat*
 570 file. In order to work, there must be a *basename.model* file in the working directory. The **generate-**
 571 **matrix** command takes six parameters which are described in Table 3. Listing 8 shows an example of the
 572 **generate-matrix** command. If successful, two files are generated: *basename.mat* and *basename.lost*.

Listing 8. The *miind.miindio* command to generate a matrix using the *adex.model* file with an efficacy of 0.1 in *v* and a jump of 5.0 in *w* when a neuron spikes. The Monte Carlo method has been chosen with 10 points per cell.

573 > generate-matrix adex 0.1 10 0.0 5.0 false

574 Once **generate-matrix** has completed, a *.mat* file will have been generated and the *.model* file will have
 575 been amended to include a *<Reset Mapping>* section. Similar to the reversal mapping in the *.rev* file,
 576 the reset mapping describes movement of probability mass from the cells which lie across the threshold
 577 potential to cells which lie across the reset potential. If the threshold or reset values are changed but no
 578 other change is made to the mesh, it can be helpful to re-run the mapping calculation without having
 579 to completely re-calculate the transition matrix. *miind.miindio* provides the command **regenerate-reset**
 580 which takes the base name and any new reset shift value (0 if not required) as parameters. This will quickly
 581 replace the reset mapping in the *.model* file.

Listing 9. The user may change the *<Threshold>* and *<Reset>* values in the *.model* file (or re-call **generate-model** with different threshold and reset values) then update the existing Reset Mapping. In this case, the *adex.model* was updated with a reset *w* shift value of 7.0.

582 > regenerate-reset adex 7.0

583 With all required files generated, a simulation using the mesh algorithm can now be run in MIIND.

584

585 3.3 Jump Files

586 In some models, it is helpful to be able to set the efficacy as a function of the state. For example,
 587 to approximate adaptive behaviour where the post synaptic efficacy lowers as the membrane potential
 588 increases. Jump files have been used in MIIND to simulate the Tsodyks-Markram (Tsodyks and Markram,
 589 1997) synapse model as described in De Kamps et al. (2019). In the model, one variable/dimension is
 590 required to represent the membrane potential, *V*, of the post-synaptic neuron and the second to represent
 591 the synaptic contribution, *G*. *G* and *V* are then used to derive the post-synaptic potential caused by an
 592 incoming spike. Before generating the transition matrix, each cell can be assigned its own efficacy for
 593 which the transitions will be calculated. During generation, Monte Carlo points will be translated according
 594 to that value instead of a constant across the entire mesh. When calling the **generate-matrix** command, a
 595 separate set of three parameters is required to use this feature. The base name of the model file, the number
 596 of Monte Carlo points per cell, and a reference to a *.jump* file which stores the efficacy values for each cell
 597 in the mesh.

Listing 10. Generate a transition matrix with a jump file in the CLI

598 > generate-matrix adex 10 adex.jump

599 As with the files required to build the mesh, the jump file must be user generated as the efficacy values may
 600 be non-linear and involve one or both of the dimensions of the model. The format of a jump file is shown
 601 in listing 11. The *<Efficacy>* element of the XML file gives an efficacy value for both dimensions of the

602 model and is how the resulting transition matrix will be referenced in the simulation. The *<Translations>*
 603 element lists the efficacy in both dimensions for each cell in the mesh.

Listing 11. The format of the jump file. Each line in the *<Translations>* block gives the strip,cell coordinates of the cell followed by the *h* efficacy then the *v* efficacy. The *<Efficacy>* element gives a reference efficacy which will be used to reference the transition matrix built with this jump file. It must therefore be unique among jump files used for the same model.

```
604 <Jump>
605 <Efficacy>0.0 0.1</Efficacy>
606 <Translations>
607 0,0 0.0 0.1
608 1,0 0.0 0.1
609 1,1 0.0 0.10012
610 1,2 0.0 0.10045
611 ...
612 </Translations>
613 </Jump>
```

614 After calling **generate-matrix**, as before, the *.mat* file will be created with the quoted values in the
 615 *<Efficacy>* element of the jump file. As with the vanilla Monte Carlo generation, the additional process of
 616 tracking lost points must be performed.

617

4 WRITING THE XML FILE

618 MIIND provides an intuitive XML style language to describe a simulation and its parameters. This includes
 619 descriptions of populations, neuron models, integration techniques, and connectivity as well as general
 620 parameters such as time step and duration. The XML file is split into sections which are sub elements of
 621 the XML root node, *<Simulation>*. They are Algorithms, Nodes, Connections, Reporting, and Simulation-
 622 RunParameter. These elements make up the major components of a MIIND simulation.

623

4.1 Algorithms

624 An *<Algorithm>* in the XML code describes the simulation method for a population in the network. The
 625 nodes of the network represent separate instances of these algorithm elements. Therefore, many nodes can
 626 use the same algorithm. Each algorithm has different parameters or supporting files but as a minimum, all
 627 algorithms must declare a type and a name. Each algorithm is also implicitly associated with a “weight
 628 type”. All algorithms used in a single simulation must be compatible with the weight type as it describes the
 629 way that populations interact. The *<WeightType>* element of the XML file can take the values, “double”,
 630 “DelayedConnection”, or “CustomConnectionParameters”. Which value the weight type element takes
 631 influences which algorithms are available in the simulation and how the connections between populations
 632 will be defined. The following sections cover all Algorithm types currently supported in MIIND. Table 4
 633 lists these algorithms and their compatible weight types.

635

4.1.1 RateAlgorithm

636 RateAlgorithm is used to supply a Poisson distributed input (with a given average firing rate) to other
 637 nodes in the simulation. It is typically used for simulating external input. The *<rate>* sub-element is used
 638 to define the activity value which is usually a firing rate.

Listing 12. A RateAlgorithm definition with a constant rate of 100Hz.

```

640 <Algorithm name="Cortical Background Algorithm" type="RateAlgorithm">
641   <rate>100.0</rate>
642 </Algorithm>
```

4.1.2 MeshAlgorithm and MeshAlgorithmCustom

644 In section 3.2, we saw how to generate *.model* and *.mat* files. These are required to simulate a population
 645 using the mesh algorithm. Algorithm type=MeshAlgorithm tells MIIND to use this technique. The model
 646 file is referenced as an attribute to the Algorithm definition. The *TimeStep* child element must match that
 647 which was used to generate the mesh. This value is quoted in the model file. As many *MatrixFile* elements
 648 can be declared as are required for the simulation, each with an associated .mat file reference.

Listing 13. A MeshAlgorithm definition with two matrix files.

```

649 <Algorithm type="MeshAlgorithm" name="ALG_ADEX" modelfile="adex.model" >
650   <TimeStep>0.001</TimeStep>
651   <MatrixFile>adex_0.05_0_0_0_.mat</MatrixFile>
652   <MatrixFile>adex_-0.05_0_0_0_.mat</MatrixFile>
653 </Algorithm>
```

654 MeshAlgorithm provides two further optional attributes in addition to *modelfile*. The first is *tau_refractive*
 655 which enables a refractory period and the second is *ratemethod* which takes the value “AvgV” if the activity
 656 of the population is to be represented by the average membrane potential. Any other value for *ratemethod*
 657 will set the activity to the default average firing rate. The activity value is what will be passed to other
 658 populations in the network as well as what will be recorded as the activity for any populations using this
 659 algorithm.

660 When the weight type is set to CustomConnectionParameters, the type of this algorithm definition should
 661 be changed to MeshAlgorithmCustom. No other changes to the definition are required.

662

4.1.3 GridAlgorithm and GridJumpAlgorithm

664 For populations which use the grid algorithm, the following listing is required. Similar to the MeshAl-
 665 gorithm, the model file is referenced as an attribute. However, there are no matrix files required as the
 666 transition matrix for solving the Poisson master equation is calculated at run time. The transition matrix
 667 for the deterministic dynamics, stored in the *.tmat* file, is referenced as an attribute as well. Attributes for
 668 *tau_refractive* and *ratemethod* are also available with the same effects as for MeshAlgorithm.

Listing 14. A GridAlgorithm definition using the AvgV (membrane potential) rate method.

```

669 <Algorithm type="GridAlgorithm" name="GRIDALG_FN" modelfile="fn.model" tau_refractive="0.0"
670   ↳ transformfile="fn_0_0_0_0_.tmat" start_v="-1.0" start_w="-0.3" ratemethod="AvgV">
671 <TimeStep>0.00001</TimeStep>
672 </Algorithm>
```

673 GridAlgorithm also provides additional attributes *start_v* and *start_w* which allows the user to set the
 674 starting state of all neurons in the population which creates an initial probability mass of 1.0 in the
 675 corresponding grid cell at the start of the simulation.

676 GridJumpAlgorithm provides a similar functionality as MeshAlgorithm when the transition matrix is
 677 generated using a jump file. That is, the efficacy applied to each cell when calculating transitions differs
 678 from cell to cell. In GridJumpAlgorithm, the efficacy at each cell is multiplied by the distance between
 679 the central *v* value of the cell and a user defined “stationary” value. The initial efficacy and the stationary

680 values are defined by the user in the XML `<Connection>` elements. GridJumpAlgorithm is useful for
 681 approximating populations of neurons with a voltage dependent synapse.

Listing 15. A GridJumpAlgorithm definition and corresponding Connection with a “stationary” attribute. The efficacy at each grid cell will equal the original efficacy value (-0.05) multiplied by the difference between each cell’s central v value and the given stationary value (-65)

```
682 <Algorithm type="GridJumpAlgorithm" name="ALG_ADEX" modelfile="adex.model" tau_refractive="0.0"
683   ↪ transformfile="adex_0_0_0_0_.tmat" start_v="-65.0" start_w="0.0">
684 <TimeStep>0.0001</TimeStep>
685 </Algorithm>
686 ...
687 <Connection In="BG_NOISE" Out="ADEX_NODE" num_connections="1" efficacy="-0.05" delay="0.0" stationary=
688   ↪ -65.0"/>
```

689 4.1.4 Additional Algorithms

690 MIIND also provides OUAlgorithm and WilsonCowanAlgorithm. The OUAlgorithm generates an
 691 Ornstein–Uhlenbeck process (Uhlenbeck and Ornstein, 1930) for simulating a population of LIF neurons.
 692 The WilsonCowanAlgorithm implements the Wilson–Cowan model for simulating population activity
 693 (Wilson and Cowan, 1972). Examples of these algorithms are provided in the examples directory of the
 694 MIIND repository (*examples/twopop* and *examples/model_archive/WilsonCowan*).
 695 One final algorithm, RateFunctor, behaves similarly to RateAlgorithm. However, instead of a rate value, the
 696 child value defines the activity using a C++ expression in terms of variable, *t*, representing the simulation
 697 time.

Listing 16. A RateFunctor algorithm definition in which the firing rate linearly increases to 100Hz over 0.1 seconds and remains at 100Hz thereafter.

```
698 <Algorithm type="RateFunctor" name="ExternalInput">
699   <expression><! [CDATA[ t < 0.1 ? (t/0.1)*100 : 100 ]]></expression>
700 </Algorithm>
```

701 A CDATA expression is not permitted when using MIIND in Python or when calling *miind.run*. However,
 702 RateFunctor can still be used with a constant expression (although this has no benefit beyond what RateAl-
 703 gorithm already provides). CDATA should only be used when MIIND is built from source (not installed
 704 using pip) and the MIIND API is used to generate C++ code from an XML file.

705

706 4.2 Nodes

707 The `<Node>` block lists instances of the Algorithms defined above. Each node represents a single
 708 population in the network. To create a node, the user must provide the name of one of the algorithms
 709 defined in the algorithm block which will be instantiated. A name must also be given to uniquely identify
 710 this node. The type describes the population as wholly inhibitory, excitatory, or neutral. The type dictates
 711 the sign of the post synaptic efficacy caused by spikes from this population. Setting the type to neutral
 712 allows the population to produce both excitatory and inhibitory (positive and negative) synaptic efficacies.
 713 For most algorithms, the valid types for a node are *EXCITATORY*, *INHIBITORY*, and *NEUTRAL*. *EXCITA-*
TORY_DIRECT and *INHIBITORY_DIRECT* are also available but mean the same as *EXCITATORY* and
 715 *INHIBITORY* respectively.

Listing 17. Three nodes defined in the Nodes section using the types *NEUTRAL*, *INHIBITORY*, and *EXCITATORY* respectively.

716 <Nodes>

```

717 ...
718 <Node algorithm="GRIDALG_FN" name="POP_1" type="NEUTRAL" />
719 <Node algorithm="ALG_ADEX" name="ADEX_NODE" type="INHIBITORY" />
720 <Node algorithm="RATEFUNC_BACKGROUND" name="BG_NOISE" type="EXCITATORY" />
721 ...
722 </Nodes>
```

723 Many nodes can reference the same algorithm to use the same population model but they will behave
 724 independently based on their individual inputs.

725

726 4.3 Connections

727 The connections between the nodes are defined in the *<Connections>* sub-element. Each connection
 728 can be thought of as a conduit which passes the output activity from the “In” population node to the “Out”
 729 population node. The format used to define the connections is dependent on the choice of *WeightType*.
 730 When the type is *double*, connections require a single value which represents the connection weight. This
 731 will be multiplied by the output activity of the In population and passed to the Out population. The sign of
 732 the weight must match the In node’s type definition (*EXCITATORY*, *INHIBITORY*, *NEUTRAL*).

Listing 18. A simple double WeightType Connection with a single rate multiplier.

```

733 <WeightType>double</WeightType>
734 <Connections>
735 ...
736 <Connection In="RATEFUNC_BACKGROUND" Out="WC_POP">0.1</Connection>
737 ...
738 </Connections>
```

739 Many algorithms use the *DelayedConnection* weight type which requires three values to define each
 740 connection. The first is the number of incoming connections each neuron in the Out population receives
 741 from the In population. This number is effectively a weight and is multiplied by the output activity of the In
 742 population. For example, if the output firing rate of an In population is 10Hz and the number of incoming
 743 connections is set to 10, the effective average incoming spike rate to each neuron in the Out population
 744 will be 100 Hz. The second value is the post synaptic efficacy whose sign must match the type of the In
 745 population. If the Out population is an instance of MeshAlgorithm, the efficacy must also match one of the
 746 provided *.mat* files. The third value is the connection delay in seconds. The delay is implemented in the
 747 same way as the refractory period in the mesh and grid algorithms. The output activity of the In population
 748 is placed at the beginning of the queue and shifted towards the end of the queue over subsequent iterations.
 749 The input to the Out population is taken as the linear interpolation between the final two values in the
 750 queue.

Listing 19. A DelayedConnection with number of connections = 10, efficacy = 0.1, and delay of 1ms.

```

751 <WeightType>DelayedConnection</WeightType>
752 <Connections>
753 ...
754 <Connection In="RATEFUNC_BACKGROUND" Out="BURSTER">10 0.1 0.001</Connection>
755 ...
756 </Connections>
```

757 With the addition of GridAlgorithm, there was a need for a more flexible connection type which would
 758 allow custom parameters to be applied to each connection. When using the *CustomConnectionParameters*

759 weight type, the key-value attributes of the connections are passed as strings to the C++ implementation.
 760 By default, custom connections require the same three values as *DelayedConnection*: *num_connections*,
 761 *efficacy*, and *delay*. *CustomConnectionParameters* can therefore be used with mesh algorithm nodes as
 762 well as grid algorithm nodes although MeshAlgorithm definitions must have the type attribute set to
 763 MeshAlgorithmCustom instead.

Listing 20. A MeshAlgorithmCustom definition for use with WeightType=CustomConnectionParameters and a Connection using the num_connections, efficacy, and delay attributes.

```
764 <WeightType>CustomConnectionParameters</WeightType>
765
766 <Algorithms>
767 ...
768 <Algorithm type="MeshAlgorithmCustom" name="ALG_ADEX" modelfile="adex.model" >
769   <TimeStep>0.001</TimeStep>
770   <MatrixFile>adex_0.05_0_0_0_.mat</MatrixFile>
771   <MatrixFile>adex_-0.05_0_0_0_.mat</MatrixFile>
772 </Algorithm>
773 ...
774 </Algorithms>
775
776
777 <Connections>
778 ...
779 <Connection In="ALG_ADEX" Out="RG_E" num_connections="1" efficacy="0.05" delay="0.0"/>
780 ...
781 </Connections>
```

782 Other combinations of attributes for connections using CustomConnectionParameters are available for
 783 use with specific specialisations of the grid algorithm which are discussed in section 4 of the supplemen-
 784 tary material. Any number of attributes are permitted but they will only be used if there is an algorithm
 785 specialisation implemented in the MIIND code base.

786 4.4 SimulationRunParameter

787 The *<SimulationRunParameter>* block contains parameter settings for the simulation as a whole. The
 788 sub-elements listed in Table 5 are required for a full definition. Although most of the sub-elements are
 789 self explanatory, *t_step* has the limitation that it must match or be an integer multiple of all time steps
 790 defined by any MeshAlgorithm and GridAlgorithm instances. *master_steps* is used only for the GPGPU
 791 implementation of MIIND (section 5). It allows the user to set the number of Euler iterations per time step to
 792 solve the master equation. By default, the value is 10. However, to improve accuracy or to avoid blow-up in
 793 the case where the time step is too large or the local dynamics are unstable, *master_steps* should be increased.
 794

795 4.5 Reporting

796 The *<Reporting>* block is used to describe how output is displayed and recorded from the simulation.
 797 There are three ways to record output from the simulation: Density, Rate, and Display. The *<Rate>*
 798 element takes the node *name* and *t_interval* as attributes and creates a single file in the output directory.
 799 *t_interval* must be greater than or equal to the simulation time step. At each *t_interval* of the simulation, the
 800 output activity of the population is recorded on a new line of the generated file. Although the element is
 801 called “Rate”, if average membrane potential has been chosen as the activity of this population, this is what

803 will be recorded here. *<Density>* is used to record the full probability density of the given population node.
 804 As density is only relevant for the population density technique, it can only be recorded from nodes which
 805 instantiate the mesh or grid algorithm types. The attributes are the node *name*, *t_start*, *t_end*, and *t_interval*
 806 which define the simulation times to start and end recording the density at the given interval. A file which
 807 holds the probability mass values for each cell in the mesh or grid will be created in the output directory
 808 for each *t_interval* between *t_start* and *t_end*. Finally, the *<Display>* element can be used to observe the
 809 evolution of the probability density function as the simulation is running. If a *Display* element is added in
 810 the XML file for a specific node, when the simulation is run, a graphical window will open and display the
 811 probability density for each time step. Again, display is only applicable to algorithms involving densities.
 812 Enabling the display can significantly slow the simulation down. However, it is useful for debugging the
 813 simulation and furthermore, each displayed frame is stored in the output directory so that a movie can be
 814 made of the node's behaviour. How to generate this movie is discussed later in section 7.1.

Listing 21. A set of reporting definitions to record the probability densities and rates of two populations, S and D. The densities will also be displayed during simulation.

```
815 <Reporting>
816 ...
817   <Density node="S" t_start="0.0" t_end="6.0" t_interval="0.01" />
818   <Density node="D" t_start="0.5" t_end="1.5" t_interval="0.001" />
819   <Display node="S" />
820   <Display node="D" />
821   <Rate node="S" t_interval="0.0001" />
822   <Rate node="D" t_interval="0.0001" />
823 ...
824 </Reporting>
```

825 4.6 Variables

826 The *<Simulation>* element can contain multiple *<Variable>* sub-elements each with a unique name
 827 and value. Variables are provided for the convenience of the user and can replace any values in the XML
 828 file. For example, a variable named *TIME_END* can be defined to replace the value in the *t_end* element of
 829 the *SimulationRunParameter* block. When the simulation is run, the value of *t_end* will be replaced with
 830 the default value provided in the Variable definition. Using variables makes it easy to perform parameter
 831 sweeps where the same simulation is run multiple times and only the variable's value is changed. How
 832 parameter sweeps are performed is covered in the supplementary material section 8. All values in a MIIND
 833 XML script can be set with a variable name. The type of the Variable is implicit and an error will be thrown
 834 if, say, a non-numerical value is passed to the *tau_refractive* attribute of a *MeshAlgorithm* object.
 835

Listing 22. A Variable definition. *TIME_END* has a default value of 18.0 and is used in the *t_end* parameter definition.

```
836 <Variable Name='TIME_END'>18.0</Variable>
837 ...
838 <t_end>TIME_END</t_end>
```

5 MIIND ON THE GPU

839 The population density techniques of the mesh and grid algorithms rely on multiple applications of the
 840 transition matrix which can be performed on each cell in parallel. This makes the algorithms prime
 841 candidates for parallelisation on the graphics card. In the CPU versions, the probability mass is stored

842 in separate arrays, one for each population/node in the simulation. For the GPGPU version, these are
 843 concatenated into one large probability mass vector so all cells in all populations can be processed in parallel.
 844 From the user's perspective, switching between CPU and GPU implementations is trivial. In the XML file
 845 for a simulation which uses MeshAlgorithm or GridAlgoirthm, to switch to the vectorised GPU version, the
 846 Algorithm types must be changed to MeshAlgorithmGroup and GridAlgorithmGroup. All other attributes
 847 remain the same. Only MeshAlgorithmGroup, GridAlgorithmGroup, and RateFunctor/RateAlgorithm
 848 types can be used for a vectorised simulation. When running a MIIND simulation containing a group
 849 algorithm from a Python script, instead of importing *miind.miindsim*, *miind.miindsimv* should be used. The
 850 Python module *miind.run* is agnostic to the use of group algorithms so can be used as shown previously.

Listing 23. A MeshAlgorithmGroup definition is identical to a MeshAlgorithm definition except for the type.

```
851 <Algorithm type="MeshAlgorithmGroup" name="ALG_ADEX" modelfile="adex.model" >
852   <TimeStep>0.001</TimeStep>
853   <MatrixFile>adex_0.05_0_0_.mat</MatrixFile>
854   <MatrixFile>adex_-0.05_0_0_.mat</MatrixFile>
855 </Algorithm>
856 <Algorithm type="GridAlgorithmGroup" name="OSC" modelfile="fn.model" tau_refractive="0.0" transformfile=
857   ↪ "fn_0_0_0_0_.tmat" start_v="-1.0" start_w="-0.3" ratemethod="AvgV">
858 <TimeStep>0.00001</TimeStep>
859 </Algorithm>
```

860 The GPGPU implementation uses the Euler method to solve the master process during each iteration. It
 861 is, therefore, susceptible to blow-up if the time step is large or if the local dynamics of the model are stiff.
 862 The user has the option to set the number of euler steps taken each iteration using the *master_steps* value of
 863 the SimulationRunParameter block in the XML file. A higher value reduces the likelihood of blow-up but
 864 increases the simulation time.

865

866 In order to run the vectorised simulations, MIIND must be running on a CUDA enabled machine and have
 867 CUDA enabled in the installation (CUDA is supported in the Windows and Linux python installations).
 868 Section 3 in the supplementary material goes into greater detail about the systems architecture differences
 869 between the CPU and GPU versions of the MIIND code. Using the “Group” algorithms is recommended if
 870 possible as it provides a significant performance increase. Benchmarking details for MIIND compared to
 871 direct simulation are available in De Kamps et al. (2019).

872

6 RUNNING A MIIND SIMULATION IN PYTHON

873 As demonstrated in the quick start guide, the command **python -m miind.run** takes a simulation XML file
 874 as a parameter and runs the simulation. A similar script may be written by the user to give more control
 875 over what happens during a simulation and how output activity is recorded and processed. It even allows
 876 MIIND simulations to be integrated into other Python applications such as the Virtual Brain (Sanz Leon
 877 et al., 2013) so the population density technique can be used to solve the behaviour of nodes in a brain-scale
 878 network (see section 9). To run a MIIND simulation in a Python script, the module *miind.miindsim* must be
 879 imported (or *miind.miindsimv* if the simulation uses MeshAlgorithmGroup or GridAlgorithmGroup and
 880 therefore requires CUDA support). Listing 24 shows an example script which uses the following available
 881 functions to control the simulation.

882

Listing 24. A simple python script for running a MIIND simulation and plotting the results.

```

883 import matplotlib.pyplot as plt
884 import miind.miindsim as miind
885
886 miind.init(1, "lif.xml")
887
888 timestep = miind.getTimeStep()
889 simulation_length = miind.getSimulationLength()
890 print('Timestep from XML : {}'.format(timestep))
891 print('Sim time from XML : {}'.format(simulation_length))
892
893 miind.startSimulation()
894
895 constant_input = [2500]
896 activities = []
897 for i in range(int(simulation_length/timestep)):
898     activities.append(miind.evolveSingleStep(constant_input)[0])
899
900 miind.endSimulation()
901
902 plt.figure()
903 plt.plot(activities)
904 plt.title("Firing Rate.")
905
906 plt.show()

```

907 6.1 init(node_count,simulation_xml_file,...)

908 The *init* function should be called first once the MIIND library has been imported. This sets up the
 909 simulation ready to be started. The *node_count* parameter allows for multiple instantiations of the simulation
 910 to be run simultaneously. The Nodes, Connections, and Reporting blocks from the simulation file will be
 911 duplicated, effectively running the same model *node_count* times simultaneously in the same simulation.
 912 This functionality was included to allow the Virtual Brain to run the simulation defined in the XML file
 913 multiple times (see section 9). The *simulation_xml_file* parameter gives the name of the simulation xml file
 914 to be run. If the file has any variables defined, these are made available in Python as additional parameters
 915 to the *init* function. In this way, the use of XML variables can be used for parameter sweeps. All variables
 916 must be passed as strings. If a variable is not set in the call to *init*, the default value defined in the XML file
 917 will be used.

Listing 25. Calling init for a MIIND simulation lif.xml with the Variable SIM_TIME set to 0.4.

```
918 miind.init(1, "lif.xml", SIM_TIME="0.4")
```

919 6.2 getTimeStep() and getSimulationLength()

920 Once *init* has been called, the functions *getTimeStep* and *getSimulationLength* can be used to extract the
 921 time step and simulation length in seconds from the simulation respectively. The Python script controls
 922 when each iteration of the MIIND simulation is called and so it needs to know the total number of iterations
 923 to make. Furthermore, it can be useful for integration with other systems to know these values.

```
924
```

925 **6.3 startSimulation()**

926 *startSimulation* indicates in the Python script that the simulation should be initialised ready for the
 927 simulation loop to be called.

928 **929 6.4 evolveSingleStep(input)**

930 By calling *evolveSingleStep* in the Python script, the MIIND simulation will move forward one time step.
 931 This function takes a list of numbers as a parameter. The list corresponds to inputs to the population nodes
 932 in the MIIND simulation. In this way, the user may control the behaviour of the simulation from the Python
 933 script during the simulation. The *evolveSingleStep* function also returns a list of numbers which are the
 934 output activities of the population nodes. Section 6.6 provides more information about how to use the input
 935 and output of this function. *evolveSingleStep* should be called in a loop which will run the same number of
 936 iterations as would be expected if the XML file were run in MIIND directly, that is, the simulation length
 937 divided by the time step.

938 **939 6.5 endSimulation()**

940 It is good practice to call *endSimulation* once all iterations of the simulation have been performed. This
 941 allows MIIND to clean up and to print the performance statistics to the console.

942 **943 6.6 Additional XML Code for Python Support**

944 Although it is still possible to use *RateFunctor* or *RateAlgorithm* to set input rates to populations in a
 945 Python MIIND simulation, *evolveSingleStep()* provides a means to pass the input rates as a parameter so
 946 that more complex input patterns can be used. In order to indicate that a population will receive input
 947 externally from the Python script (via the list input to *evolveSingleStep()*) a special connection type must
 948 be defined in the *<Connections>* section of the XML.

Listing 26. Special connection types for use in Python.

```
949 <Connections>
950 ...
951 <IncomingConnection Node="E">1 0.01 0</IncomingConnection>
952 <OutgoingConnection Node="E"/>
953 ...
954 </Connections>
```

955 Listing 26 defines an input to node E which will be interpreted as a *DelayedConnection* with the number
 956 of connections equal to 1 and a post synaptic efficacy of 0.01. No delay is defined here although it is
 957 permitted. *OutgoingConnections* are used to declare which nodes in the population network will pass their
 958 activity back to the Python script after each iteration. If the two connections in the listing are the only
 959 instances of *IncomingConnection* and *OutgoingConnection*, then the *evolveSingleStep* function will expect
 960 as a parameter, a list with one numeric value to represent the incoming rate to node E. *evolveSingleStep*
 961 will return a list with a single numeric value representing the activity of node E. In cases where there are
 962 more than one *IncomingConnection*, the order of values in the Python list parameter to *evolveSingleStep* is
 963 the same as the order of *IncomingConnections* defined in the XML. Similarly with *OutgoingConnections*,
 964 the order of the list of activities returned from *evolveSingleStep* is the same as the order of declaration in
 965 the XML file.

7 USING THE CLI TO QUICKLY VIEW RESULTS

966 Once a simulation has been run, either using *miind.run* or from a user written Python script, the
967 *miind.miindio* CLI can be used to quickly plot the recorded results. As mentioned, the commands used
968 in *miindio* are based on the module *miind.miind_api* and are reproducible in a Python script. However, it
969 can be convenient to be able to run them directly from the command line to aid fast prototyping and bug
970 fixing of models and simulations. The following section lists some common commands in the CLI and
971 their usage. The accompanying files for this example are in the *examples/cli_plots* directory. The following
972 command starts the CLI and presets the user with a prompt:

Listing 27. Run the CLI.

973 \$ python -m miind.miindio

974 When *miind.miindio* is called for the first time in a working directory, the user must identify the XML file
975 which will describe the current working simulation. MIIND stores a reference to this file in a settings file in
976 the working directory so that all subsequent commands will reference this simulation. Even if *miind.miindio*
977 is quit and restarted, the current working simulation will be used as the context for commands until a new
978 current working simulation is defined or if it is called in a different directory. The user can set the current
979 working simulation with the **sim** command.
980

Listing 28. Load a simulation file in the CLI.

981 > sim example.xml

982 Calling **sim** without a parameter will list information about the current working simulation such as the
983 output directory, XML file name and provide a list of the defined variables and nodes.
984

985 During the simulation, MIIND generates output files according to the requirements of the *<Recording>*
986 object of the XML file which could include the average firing rate of population nodes or their densities at
987 each time interval. The average firing rate can be plotted from the CLI using the **rate** command followed by
988 the name of the population node. To be reminded of the node names, the user can call **sim** or **rate** without
989 parameters.
990

Listing 29. Plot the rate of population POP1 in the CLI.

991 > rate POP1

992 Even while a simulation is running, calling **rate** in the CLI will plot the recorded activity up to the latest
993 simulated time point. This is useful to keep an eye on the simulation as it progresses without waiting for
994 completion. An example of the plots produced by **rate** is shown in Fig. 11A.
995 For populations using the grid or mesh algorithms, the user can call the **plot-density** command with
996 parameters identifying the required node name and simulation time.
997

Listing 30. Plot the probability density of population POP1 at time 0.42s in the CLI.

998 > plot-density POP1 0.42

999 This command renders the mesh or grid and its population density at the given simulation time. When
1000 reading the simulation time parameter in the command, MIIND expects the time to be an integer multiple

1001 of the time step and to be expressed up to its least significant figure (for example, 0.1 instead of 0.10).
 1002 Again, this command can be run during a simulation providing the time has been simulated. An example of
 1003 a density plot is shown in Fig. 11B.

1004

1005 Similar to **plot-density**, **plot-marginals** can be used to display the marginal densities of a given popula-
 1006 tion at a given time. Both marginals are plotted next to each other. The details of how marginal densities are
 1007 calculated are explained in the supplementary material section 5. Fig. 11C shows an example of a marginal
 1008 density plot.

1009

Listing 31. Plot the marginal distributions of population POP1 at time 0.42s in the CLI.

1010 > plot-marginals POP1 0.42

1011 7.1 Generate a Density Movie

1012 If, in the XML file *<Recording>* section, the *<Display>* element is added for a given population, the
 1013 output directory will be populated with still images of density plots at each time step. Once the simulation
 1014 is complete, calling **generate-density-movie** in the CLI will produce an MP4 movie file made from the
 1015 still images. The parameters are the node name followed by the size of the square video frame in pixels.
 1016 The third parameter is the desired time to display each image (every time step of the simulation) in seconds.
 1017 If the video should be the same length as the simulation time, then this parameter should match the time
 1018 step of the simulation. By changing the value, the video time can be altered. For example, if the parameter
 1019 is set to 0.01 for a simulation with time step 0.001, then the video length will be 10 times the length of the
 1020 simulation. Finally, a name for the video file must be given.

Listing 32. Generate a movie from the display images of population POP1 with a size of 512 pixels at a
 simulation replay time step of 0.1s.

1021 > generate-density-movie POP1 512 0.1 pop1_mov

1022 The movie file will be created in the working directory of the simulation. A movie of the marginal density
 1023 plots can also be created using the **generate-marginal-movie** command which takes the same parameters.
 1024 As each marginal plot must be generated from the density output, this takes a considerably longer time
 1025 than for the density movie.

Listing 33. Generate a marginals movie from the density files of population POP1 with a size of 512
 pixels at a simulation replay time step of 0.1s.

1026 > generate-marginal-movie POP1 512 0.1 pop1_marginal_mov

8 DESCRIPTION OF MIIND'S ARCHITECTURE AND FUNCTIONALITY

1027 The main architectural concerns in MIIND relate to the two C++ libraries, MPILib and TwoDLib. MPILib
 1028 is responsible for instantiating and running the simulation. TwoDLib contains the CPU implementations of
 1029 the grid and mesh algorithms. It is also responsible for generating transition matrices. Of the remaining
 1030 libraries, GeomLib contains a population density technique implementation of neuron models with one
 1031 time dependent variable, although it is also possible and indeed preferable to use the TwoDLib code for
 1032 one dimensional models. EPFLlib and NumtoolsLib contain helper classes and type definitions. Fig. 12
 1033 shows a reduced UML diagram of the MIIND C++ architecture. The aim of this section is to give a brief
 1034 overview of the C++ MIIND code as a starting point for developers. The CUDA implementation of MIIND
 1035 is similar in structure to the CPU solution and is available in the CudaTwoDLib and MiindLib libraries. A

1036 description of the differences is given in section 3 of the supplementary material.

1037 8.1 MPILib

1039 The MPINetwork class in MPILib represents a simulation as a whole and is instantiated in the *init* function
1040 of the SimulationParserCPU class which is a specialisation of MiindTvbModelAbstract. *init* is called from
1041 the Python module and, as the name suggests, MiindTvbModelAbstract was originally written with the aim
1042 of Python integration into TVB. MPINetwork exposes member functions for building a network of nodes
1043 where each node is an instance of a neuron population which can be connected together so that the output
1044 activity from one population is input to another. The class also contains all of the simulation parameters
1045 such as the simulation length and time step. Finally, the MPINetwork class exposes a function to run the
1046 simulation in its entirety or take a single evolve step for use in an external control loop.

1047

1048 Each node in the population network is represented by an instance of the MPINode class. A node
1049 has a name and an ID which is used to uniquely identify it in the simulation. A node also contains an
1050 implementation of AlgorithmInterface performing the integration technique required for this population
1051 (for example, GridAlgorithm or MeshAlgorithm). The *NodeType* describes whether a population should be
1052 thought of as excitatory or inhibitory. As discussed earlier, MIIND performs a validation check that the
1053 synaptic efficacy from a node is positive or negative respectively (or neutral). During each iteration, each
1054 node is responsible for consolidating the activity of all input connections, calling the integration step in the
1055 AlgorithmInterface implementation, and reporting the density and output activity (the average firing rate or
1056 membrane potential).

1057

1058 In MPILib, a number of implementations of AlgorithmInterface are defined which can be instantiated
1059 in a node. Implementations of AlgorithmInterface are responsible for the lion’s share of the computation
1060 in MIIND as this is where the integration of the model is performed. The interface is extremely simple,
1061 providing a function to set parameters, an optional function for a preamble before each iteration, and
1062 the *evolveNodeState* function to be called every time step. GridAlgorithm and MeshAlgorithm are imple-
1063 mentations of this interface defined in TwoDLib. MPILib and GeomLib hold the implementations of the
1064 remaining algorithms available to the user which were discussed in section 4. Finally, the weight types,
1065 DelayedConnection and CustomConnectionParameters are also defined in MPILib. All classes are C++
1066 templates which take the weight type as a parameter to avoid code duplication and to enforce that only
1067 algorithms with the same weight type can be used together.

1068 8.2 TwoDLib

1070 As with the population models in MPILib and GeomLib, GridAlgorithm and MeshAlgorithm are imple-
1071 mentations of the AlgorithmInterface. We will focus here on the grid algorithm implementation although
1072 the mesh algorithm uses the same structures or specialisations of those structures to perform similar tasks
1073 as set out in section 3. GridAlgorithm is supported by two important classes. **Ode2DSys** transfers
1074 probability mass according to the reset mapping of the *.model* file and calculates the average firing rate of
1075 the population. In MeshAlgorithm, Ode2DSys also performs the pointer update for shifting probability
1076 mass down the strips of the mesh. **MasterGrid** is responsible for solving the Poisson master equation using
1077 a transition matrix calculated at simulation time based on the desired efficacy and grid cell size. For each
1078 iteration, the function *evolveNodeState* is called which performs the main steps of the population density

1079 algorithm.

1080

1081 First, in GridAlgorithm, the deterministic dynamics are solved by applying the pre-generated transition
1082 matrix once. The second step is a call to *Ode2DSys*.*RedistributeProbability()* to perform any reset
1083 mappings for probability mass which appeared in the threshold cells last iteration. This step is useful for
1084 neuron models, such as leaky integrate and fire, which contain an instruction to reset one or more variables
1085 to a different value upon reaching a threshold.

1086

1087 The third step calls on the MasterGrid class to solve the master equation for the incoming Poisson spike
1088 rates from every incident node. MasterGrid begins with the current state of the probability mass distribution
1089 across the grid, that is, the probability mass values of each cell in the grid. As described in section 2, every
1090 cell has the same relative transition of probability mass due to a single incoming spike. For the whole
1091 grid, this single transition is duplicated into a transition matrix which can be applied to the full probability
1092 mass vector. Because there are at most two cells into which probability mass is transferred, this matrix
1093 is extremely sparse and can be stored efficiently in a compressed sparse row (CSR) matrix. In the mesh
1094 algorithm, this matrix is loaded from the .mat file.

1095

1096 MeshAlgorithm requires a fourth step to transfer probability mass from the ends of strips to stationary
1097 cells subject to a reversal mapping generated during the pre-processing phase. This is discussed in the
1098 supplementary material section 6.

1099

1100 Finally, SimulationParserCPU is an extension of the MiindTvbModelAbstract class used to parse the
1101 simulation XML file and instantiate an MPINetwork object with the appropriate nodes and connections. Its
1102 extensions of the functions declared in MiindTvbModelAbstract are exposed to the Python module to be
1103 called from a Python script.

9 DISCUSSION

1104 **MIIND fulfills a need for insight into neural behaviour at mesoscopic scales.**

1105 The MIIND population density technique allows researchers to simulate population level behaviour by
1106 defining the behaviour of the underlying neurons. This is in contrast to many rate based models which
1107 describe the population behaviour directly. An example of how population behaviour can differ from the
1108 underlying neuron model can be seen in the behaviour of a population of bursting neurons such as the
1109 Izhikevich simple model. A single Izhikevich neuron with a constant input current or input spike rate
1110 oscillates between a bursting period of repeated firing and a quiescent period of no firing. The average
1111 behaviour of a population of Izhikevich neurons is different. Initially, all neurons are synchronised, they
1112 burst and quiesce at the same time producing an oscillatory pattern of average firing rate in the population.
1113 However, due to the random nature of Poisson input spikes, the neurons de-synchronise over time and the
1114 average firing rate of the whole population damps to a constant value because only a subset of neurons
1115 are bursting at any one time. Fig. 11A shows the damping of the output firing rate oscillations and the
1116 ‘desynchronised’ density of a population of Izhikevich simple neurons.

1117

1118 TVB Integration

1119 The Virtual Brain (Sanz Leon et al., 2013) and MIIND are both systems which facilitate the development
1120 of neural mass or mean field population models with explicit descriptions of how multiple populations are
1121 connected. Using these systems, the complex dynamics arising from the interaction of populations can be
1122 studied.

1123 TVB provides a framework to describe a network of nodes (the connectivity) which, while it can be abstract,
1124 generally represents regions of the human or primate brain. Connections between nodes represent white
1125 matter tracts which transfer signals from one node to the next based on length and propagation speed. TVB
1126 also allows the description of “coupling” functions which modulate these signals as they pass from one
1127 node to another. Typically, the number of nodes is in the order of 100 or so. However, TVB also allows for
1128 the definition of a “surface” which can be associated with 10s of thousands of nodes to simulate output
1129 from common medical recording techniques such as EEG and BOLD fMRI. TVB has impressive clinical
1130 relevance as well as supporting more theoretical neuroscience research. Users can build simulations using
1131 the graphical user interface or directly using the Python source code.
1132

1133 While MIIND and TVB have many functional similarities, both have differing strengths with respect to
1134 the underlying simulation techniques and surrounding infrastructure. It was therefore clear that integrating
1135 the smaller system, MIIND, into the more developed infrastructure of TVB might yield benefits from both.
1136

1137 Although it is possible to model delayed connections and synaptic dynamics between populations in
1138 MIIND, TVB provides a comprehensive method of defining such structures and behaviours through the
1139 connectivity network and coupling functions. Some users of MIIND may find it useful and appropriate to
1140 house their simulations in such a structure.
1141

1142 TVB uses a number of model classes to describe the behaviour of the nodes in a network. When the
1143 simulation is run, an instantiation of a specified model class takes the signals which have passed through
1144 the network to arrive at each node and integrates forward by one time step (depending on the integration
1145 method). In order to use MIIND nodes in TVB, a specialised model class was created to import the MIIND
1146 Python library, instantiate it, then make a call to *evolveSingleStep()* in place of the integration function. The
1147 inputs and outputs of *evolveSingleStep()* are treated by TVB as any other model. As the MIIND Python
1148 library takes a simulation file name as a parameter to its *init* function, a single additional model class is all
1149 that is required to expose any MIIND simulation to TVB. Fig. 13 shows the results from a simulation of
1150 the TVB default whole-brain connectivity with populations of Izhikevich simple neurons in MIIND. The
1151 script and simulation files are available in the *examples/miind_tvb* directory of the MIIND repository. Both
1152 TVB and MIIND must be installed to sucessfully run the example.
1153

**1154 Reasoning about probability density instead of populations of individual neurons
1155 simplifies output analysis.**

1156 The output firing rate or membrane potential of a MIIND population which uses the the mesh algorithm
1157 or grid algorithm is devoid of any variation which you would see from a population of individual neurons.
1158 This is because the effect of Poisson generated input spike trains is applied to a probability density function,
1159 effectively an infinite population of neurons. Spike train inputs to a finite population of neurons produces
1160 variation in how individual neurons move through state space resulting in noisy output rates at the popula-
1161 tion level. While this can be mitigated using a larger number of neurons, the use of smoothing techniques,

1162 or curve fitting, MIIND requires none of these methods to produce an output which is immediately clear to
1163 interpret. For example, MIIND was used to build and simulate a spinal circuit model using populations
1164 of integrate and fire neurons (York et al., 2019). The average firing rates of the populations were used to
1165 compare patterns of activity with results from an EMG experiment. As the patterns to be observed were
1166 on the order of seconds, there was no need to capture faster variation in activity from the simulation and
1167 indeed, a direct simulation would have produced output which may have obscured these patterns.
1168

1169 MIIND has also been used to simulate central pattern generator models which rely on mutually inhibiting
1170 populations of bursting neurons. The interaction of the two populations significantly influences their sub-
1171 threshold dynamics. In particular, it can be difficult to identify the dynamics responsible for the swapping
1172 of states from bursting to quiescent (escape or release). Observing the changing probability density function
1173 during the simulation makes it very clear how the two populations are behaving.

1174 **Handling Noise**

1176 A major benefit of MIIND’s population density technique is the ability to observe the effect of noise on a
1177 population, and to manipulate noise in an intuitive way. For a given simulation, the Poisson distributed
1178 input to a population causes a spread of probability mass across the state space as some neurons receive
1179 many spikes, and some receive fewer. It is explained in de Kamps (2013) how the Poisson input causes a
1180 mean increase in membrane potential equal to the product of the post synaptic efficacy, h , and the average
1181 input rate, ν . It causes a variance equal to νh^2 . h and ν can therefore be set such that the mean remains the
1182 same but the variance changes to observe the effect of noise on the population.
1183

1184 Another simple way to increase the variance of the population is to introduce two additional inputs with
1185 equal rates and opposite post-synaptic efficacies. Again, the mean increase caused by the input remains
1186 unchanged but the variance can be increased significantly and this requires only a small change to the XML
1187 simulation file.

1188 **A model agnostic system at the population level makes prototyping quick and intuitive.**

1190 Because MIIND provides insight of how a neuron model produces behaviour at the population level, it is
1191 beneficial that the grid algorithm enables the user to quickly reproduce the *.model* and *.tmat* files if the
1192 underlying neuron model needs to be changed. An example of this can be observed in a half-centre oscillator
1193 made of a pair of mutually inhibiting populations of bursting neurons. The frequency of oscillation can be
1194 made dependent or independent of the input spike rate by including a limit on the slow excitability variable
1195 of the underlying neuron model. To make this change, the user can alter the neuron model then rebuild the
1196 *.model* and *.tmat* file and no change to the population level network is required.
1197

DipDE

1199 DipDE (DiPDE, 2015; Iyer et al., 2013) is an alternative implementation of the population density
1200 technique for one dimensional neuron models. It does not employ the “mesh” discretisation method used
1201 in the MIIND mesh algorithm and has primarily been used with populations of leaky integrate and fire
1202 neurons. DiPDE can be used to simulate the Potjans-Diesmann microcircuit model (Cain et al., 2016)
1203 which shows good agreement with MIIND (Fig. 5). MIIND is a much larger application than DiPDE
1204 because it allows users to design their own underlying neuron models for each population using either the

1205 mesh or grid algorithms.

1206

1207 Future Work

1208 A limitation on the MIIND population density technique is that a maximum of two time-dependent
1209 variables can be used to describe the underlying neuron model of each population. In the mesh algorithm,
1210 for higher dimensions, mesh building would need to be automated but this is not a trivial problem to solve.
1211 The grid algorithm, however, is entirely automated and work has been done to extend MIIND for 3D
1212 neuron models. Fig. 14 shows the 3D density plot of a population of Hindmarsh-Rose neurons in MIIND.
1213 The technique used to generate the 2D transition matrices outlined in section 2 extends to N dimensions so
1214 there is theoretically no limit to the dimensionality of the underlying neuron model in the grid algorithm.
1215 However, both the grid algorithm and mesh algorithm suffer from “the curse of dimensionality” such that
1216 with each additional variable, the number of cells to cover the state space increases to the point where the
1217 memory and processing requirements are too high. Luckily, a great number of neuron behaviours can be
1218 captured with only two or three time-dependent variables with appropriate approximations.

1219

1220 Large networks can be built up quickly in MIIND. To add a node to a simulation file requires just a
1221 single line. Integrating the node into the rest of the network with requisite connections is equally convenient.
1222 As mentioned, the Potjans-Diesmann model has been implemented as a single cortical column but this is
1223 by no means the limit of the size of network which can be built. It is feasible that a patch of cortex made of
1224 perhaps hundreds of cortical columns can be simulated efficiently in MIIND. The benefit of such a network
1225 would be to demonstrate how cortical columns interact together under different connectivity regimes and
1226 inputs as well as providing the ability to quickly and easily “swap out” the underlying neuron model of
1227 each population. Typically, LIF is used but adaptive integrate and fire would be a closer approximation to
1228 pyramidal neurons in cortex.

1229

1230 Conclusion

1231 We have reintroduced MIIND’s population density techniques for simulating populations of neurons
1232 and given a full account of the features available to users. While the mesh algorithm was developed some
1233 time ago, the grid algorithm which was added to MIIND recently has precipitated a more accessible, user
1234 friendly software package. We hope that the explanations given here along with a lower technical barrier to
1235 entry will encourage researchers to make use of the tool.

CONFLICT OF INTEREST STATEMENT

1236 The authors declare that the research was conducted in the absence of any commercial or financial
1237 relationships that could be construed as a potential conflict of interest.

AUTHOR CONTRIBUTIONS

1238 HO and MdK contributed to the text of this article. YML, MEL, DS, and LD contributed to the development
1239 of the population density technique and MIIND software.

1240

FUNDING

1241 This project received funding from the European Union’s Horizon 2020 research and innovation programme
1242 under Grant Agreement No. 720270 (HBP SGA1) and Specific Grant Agreement No. 785907 (Human

1243 Brain Project SGA2) (MdK; YML). HO is funded by EPSRC. The funders had no role in study design,
1244 data collection and analysis, decision to publish, or preparation of the manuscript.

ACKNOWLEDGMENTS

1245 The authors wish to thank Frank van der Velde and Martin Perez-Guevara for their continued support of
1246 the MIIND project.

DATA AVAILABILITY STATEMENT

1247 The MIIND source code and installation packages are available as a github repository at <https://github.com/dekamps/miind>.
1248 MIIND can be installed for use in Python using “pip install miind” on many Linux, MacOS, and Windows
1249 machines with python versions ≥ 3.6 .
1251 Documentation is available at <https://miind.readthedocs.io/>.

REFERENCES

- 1252 Amit, D. J. and Brunel, N. (1997). Model of global spontaneous activity and local structured activity
1253 during delay periods in the cerebral cortex. *Cerebral cortex (New York, NY: 1991)* 7, 237–252
- 1254 Bower, J. M. and Beeman, D. (2012). *The book of GENESIS: exploring realistic neural models with the*
1255 *GEneral NEural SImulation System* (Springer Science & Business Media)
- 1256 Brette, R. and Gerstner, W. (2005). Adaptive exponential integrate-and-fire model as an effective description
1257 of neuronal activity. *Journal of neurophysiology* 94, 3637–3642
- 1258 Brunel, N. and Hakim, V. (1999). Fast global oscillations in networks of integrate-and-fire neurons with
1259 low firing rates. *Neural computation* 11, 1621–1671
- 1260 Cain, N., Iyer, R., Koch, C., and Mihalas, S. (2016). The computational properties of a simplified cortical
1261 column model. *PLoS computational biology* 12, e1005045
- 1262 Carlu, M., Chehab, O., Dalla Porta, L., Depannemaeker, D., Héricé, C., Jedynak, M., et al. (2020). A
1263 mean-field approach to the dynamics of networks of complex neurons, from nonlinear integrate-and-fire
1264 to hodgkin-huxley models. *Journal of neurophysiology* 123, 1042–1051
- 1265 D’Angelo, E., Antonietti, A., Casali, S., Casellato, C., Garrido, J. A., Luque, N. R., et al. (2016). Modeling
1266 the cerebellar microcircuit: new strategies for a long-standing issue. *Frontiers in cellular neuroscience*
1267 10, 176
- 1268 de Kamps, M. (2013). A generic approach to solving jump diffusion equations with applications to neural
1269 populations. *arXiv preprint arXiv:1309.1654*
- 1270 De Kamps, M., Lepperød, M., and Lai, Y. M. (2019). Computational geometry for modeling neural
1271 populations: From visualization to simulation. *PLoS computational biology* 15, e1006729
- 1272 De Kamps, M., Lepperød, M., Lai, Y. M., and Osborne, H. (2020). *MIIND : Multiple Instantiations of*
1273 *Interacting Neural Dynamics* [Internet]. Available from: <http://miind.sourceforge.net>.
- 1274 DiPDE (2015). Website: © 2015 Allen Institute for Brain Science. *DiPDE Simulator* [Internet]. Available
1275 from: <https://github.com/AllenInstitute/dipde>.
- 1276 El Boustani, S. and Destexhe, A. (2009). A master equation formalism for macroscopic modeling of
1277 asynchronous irregular activity states. *Neural computation* 21, 46–100
- 1278 FitzHugh, R. (1961). Impulses and physiological states in theoretical models of nerve membrane.
1279 *Biophysical journal* 1, 445

- 1280 Fourcaud-Trocmé, N., Hansel, D., Van Vreeswijk, C., and Brunel, N. (2003). How spike generation
1281 mechanisms determine the neuronal response to fluctuating inputs. *Journal of Neuroscience* 23, 11628–
1282 11640
- 1283 Furber, S., Galluppi, F., Temple, S., and Plana, L. (2014). The spinnaker project. *IEEE. Proceedings* 102,
1284 652–665. doi:10.1109/JPROC.2014.2304638
- 1285 Gerstner, W. (1998). *Spiking neurons*. Tech. rep., MIT-press
- 1286 Gewaltig, M.-O. and Diesmann, M. (2007). Nest (neural simulation tool). *Scholarpedia* 2, 1430
- 1287 Hindmarsh, J. L. and Rose, R. (1984). A model of neuronal bursting using three coupled first order
1288 differential equations. *Proceedings of the Royal society of London. Series B. Biological sciences* 221,
1289 87–102
- 1290 Hines, M. L. and Carnevale, N. T. (2001). Neuron: a tool for neuroscientists. *The neuroscientist* 7, 123–135
- 1291 Iyer, R., Menon, V., Buice, M., Koch, C., and Mihalas, S. (2013). The influence of synaptic weight
1292 distribution on neuronal population dynamics. *PLoS Comput Biol* 9, e1003248
- 1293 Izhikevich, E. M. (2003). Simple model of spiking neurons. *IEEE Transactions on neural networks* 14,
1294 1569–1572
- 1295 Izhikevich, E. M. (2007). *Dynamical systems in neuroscience* (MIT press)
- 1296 Jirsa, V. K., Stacey, W. C., Quilichini, P. P., Ivanov, A. I., and Bernard, C. (2014). On the nature of seizure
1297 dynamics. *Brain* 137, 2210–2230
- 1298 Kamps, M. d. (2003). A simple and stable numerical solution for the population density equation. *Neural
1299 computation* 15, 2129–2146
- 1300 Knight, B. W. (1972). Dynamics of encoding in a population of neurons. *The Journal of general physiology*
1301 59, 734–766
- 1302 Knight, B. W., Manin, D., and Sirovich, L. (1996). Dynamical models of interacting neuron populations in
1303 visual cortex. *Robot Cybern* 54, 4–8
- 1304 Lai, Y. M. and de Kamps, M. (2017). Population density equations for stochastic processes with memory
1305 kernels. *Physical Review E* 95, 062125
- 1306 Mattia, M. and Del Giudice, P. (2002). Population dynamics of interacting spiking neurons. *Physical
1307 Review E* 66, 051917
- 1308 Mattia, M. and Del Giudice, P. (2004). Finite-size dynamics of inhibitory and excitatory interacting spiking
1309 neurons. *Physical Review E* 70, 052903
- 1310 Montbrió, E., Pazó, D., and Roxin, A. (2015). Macroscopic description for networks of spiking neurons.
1311 *Physical Review X* 5, 021028
- 1312 Nagumo, J., Arimoto, S., and Yoshizawa, S. (1962). An active pulse transmission line simulating nerve
1313 axon. *Proceedings of the IRE* 50, 2061–2070
- 1314 Nykamp, D. Q. and Tranchina, D. (2000). A population density approach that facilitates large-scale
1315 modeling of neural networks: Analysis and an application to orientation tuning. *Journal of computational
1316 neuroscience* 8, 19–50
- 1317 Omurtag, A., Knight, B. W., and Sirovich, L. (2000). On the simulation of large populations of neurons.
1318 *Journal of computational neuroscience* 8, 51–63
- 1319 Potjans, T. C. and Diesmann, M. (2014). The cell-type specific cortical microcircuit: relating structure and
1320 activity in a full-scale spiking network model. *Cerebral cortex* 24, 785–806
- 1321 Proix, T., Bartolomei, F., Guye, M., and Jirsa, V. K. (2017). Individual brain structure and modelling
1322 predict seizure propagation. *Brain* 140, 641–654
- 1323 Sanz Leon, P., Knock, S. A., Woodman, M. M., Domide, L., Mersmann, J., McIntosh, A. R., et al. (2013).
1324 The virtual brain: a simulator of primate brain network dynamics. *Frontiers in neuroinformatics* 7, 10

- 1325 Traub, R. D., Contreras, D., Cunningham, M. O., Murray, H., LeBeau, F. E., Roopun, A., et al. (2005).
1326 Single-column thalamocortical network model exhibiting gamma oscillations, sleep spindles, and
1327 epileptogenic bursts. *Journal of neurophysiology* 93, 2194–2232
- 1328 Tsodyks, M. V. and Markram, H. (1997). The neural code between neocortical pyramidal neurons depends
1329 on neurotransmitter release probability. *Proceedings of the national academy of sciences* 94, 719–723
- 1330 Uhlenbeck, G. E. and Ornstein, L. S. (1930). On the theory of the brownian motion. *Physical review* 36,
1331 823
- 1332 Wilson, H. R. and Cowan, J. D. (1972). Excitatory and inhibitory interactions in localized populations of
1333 model neurons. *Biophysical journal* 12, 1–24
- 1334 Wilson, M. A., Bhalla, U. S., Uhley, J. D., and Bower, J. M. (1988). Genesis: a system for simulating
1335 neural networks
- 1336 York, G., Osborne, H., Sriya, P., Astill, S., De Kamps, M., and Chakrabarty, S. (2019). Muscles recruited
1337 during an isometric knee extension task is defined by proprioceptive feedback. *BioRxiv* , 802736

TABLES

Table 1. Parameters for the `grid_generate.generate` function.

Parameter Name	Notes
<code>func</code>	The underlying neuron model function.
<code>timestep</code>	The desired time step for the neuron model
<code>timescale</code>	A scale factor for the timescale of the underlying neuron model to convert the time step into seconds.
<code>tolerance</code>	An error tolerance for solving a single time step of the neuron model.
<code>basename</code>	The base name with which all output files will be named.
<code>threshold_v</code>	The spike threshold value for integrate and fire neuron models.
<code>reset_v</code>	The reset value for integrate and fire neuron models.
<code>reset_shift_h</code>	A value for increasing the second variable during reset for integrate and fire neuron models with some adaptive shift or similar function.
<code>grid_v_min</code>	The minimum value for the first dimension of the grid (usually membrane potential).
<code>grid_v_max</code>	The maximum value for the first dimension of the grid.
<code>grid_h_min</code>	The minimum value for the second dimension of the grid.
<code>grid_h_max</code>	The maximum value for the second dimension of the grid.
<code>grid_v_res</code>	The number of columns in the grid.
<code>grid_h_res</code>	The number of rows in the grid.
<code>efficacy_orientation</code>	The direction, ‘v’ or ‘h’, in which incoming spikes cause an instantaneous change.

Table 2. Parameters for the `generate-model` command in the CLI.

Parameter Name	Notes
<code>basename</code>	The shared name of the <code>.mesh</code> , <code>.stat</code> , <code>.rev</code> and generated <code>.model</code> files.
<code>reset</code>	The value (usually representing membrane potential) which probability mass will be transferred to having passed the threshold.
<code>threshold</code>	The value (usually representing membrane potential) beyond which probability mass will be transferred to the reset value.

Table 3. Parameters for the `generate-matrix` command in the CLI.

Parameter Name	Notes
<i>basename</i>	The shared name of the <code>.model</code> , <code>.fid</code> (if required), and generated <code>.mat</code> files.
<i>v_efficacy</i>	The efficacy value in the <i>v</i> (membrane potential) direction. If the parameter <i>h_efficacy</i> is used, this should be zero.
<i>points / precision</i>	For Monte Carlo, this gives the number of points per cell to use for approximating the transition matrix. For the geometric method, transitions are stored in the <code>.mat</code> file to the nearest $\frac{1}{precision}$
<i>h_efficacy</i>	The efficacy value in the <i>h</i> direction. If the parameter <i>v_efficacy</i> is used, this should be zero.
<i>reset-shift</i>	The shift in the <i>h</i> direction which neurons take when being reset.
<i>use_geometric</i>	A boolean flag set to “true” if the geometric method is used and “false” for Monte Carlo.

Table 4. Compatible weight types for each algorithm type defined in the simulation XML file.

Algorithm Name	double	DelayedConnection	CustomConnectionParameters
<i>RateAlgorithm</i>	✓	✓	✓
<i>MeshAlgorithm</i>		✓	
<i>MeshAlgorithmCustom</i>			✓
<i>GridAlgorithm</i>			✓
<i>GridJumpAlgorithm</i>			✓
<i>OUAlgorithm</i>		✓	✓
<i>WilsonCowanAlgorithm</i>	✓		
<i>RateFunctor</i>	✓	✓	✓

Table 5. The required sub-elements for the `SimulationRunParameter` section of the XML simulation file.

Element	Notes
<i>SimulationName</i>	The name of the simulation.
<i>t_end</i>	The simulation end time.
<i>t_step</i>	The time step of the simulation.
<i>name_log</i>	A file name for logging. The file is stored in the output directory of the simulation.
<i>master_steps</i>	The number of Euler iterations per time step used to solve the master equation in the GPGPU implementation.

FIGURES

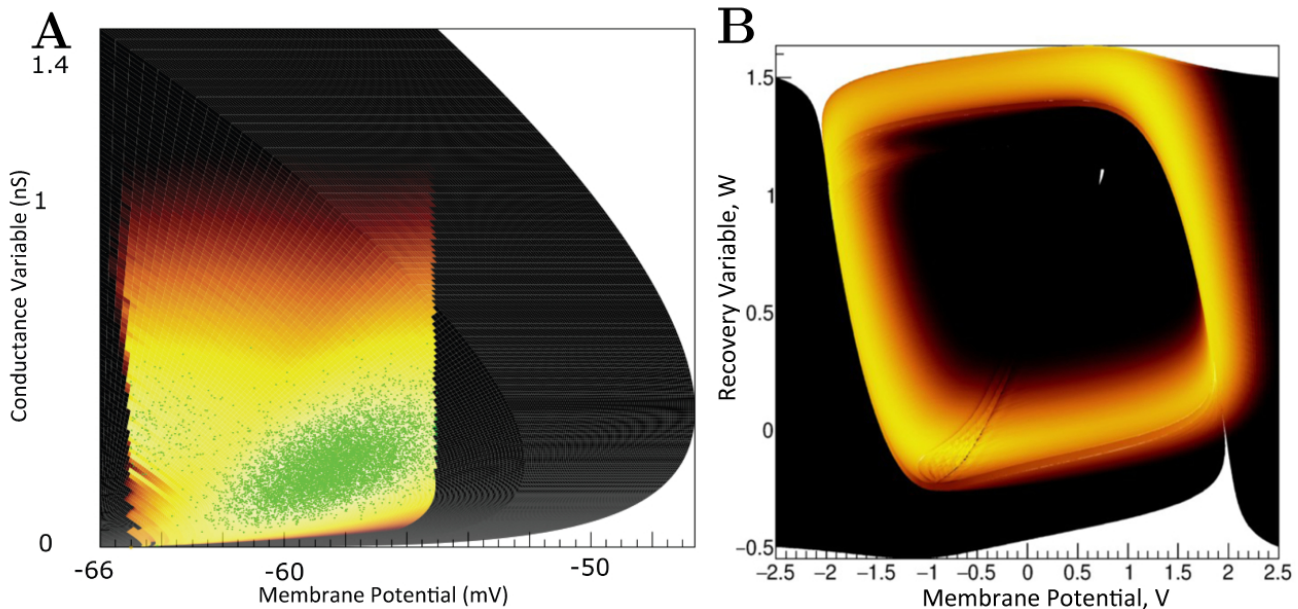


Figure 1. (A) The state space of a conductance based point model neuron. It is spanned by two variables: the membrane potential and a variable representing how open the channel is. This channel has an equilibrium potential that is positive. The green dots represent the state of individual neurons in a population. They are the result of the direct simulation of a group of neurons. MIIND, however, produces the heat plot representing a density which predicts where neurons in the population are likely to be: most likely in the white areas, least likely in the red areas and not at all in the black areas. The sharp vertical cut of the coloured area at -55mV represents the threshold at which neurons are removed from state space. They are subsequently inserted at the reset potential, at their original conductance state value. (B) The state space of a Fitzhugh-Nagumo neuron model. The axes have arbitrary units for variables V and W . There is no threshold-reset mechanism and the density follows a limit cycle. After a certain amount of simulation time, neurons can be found at all points along the limit cycle as shown here by a consistently high brightness.

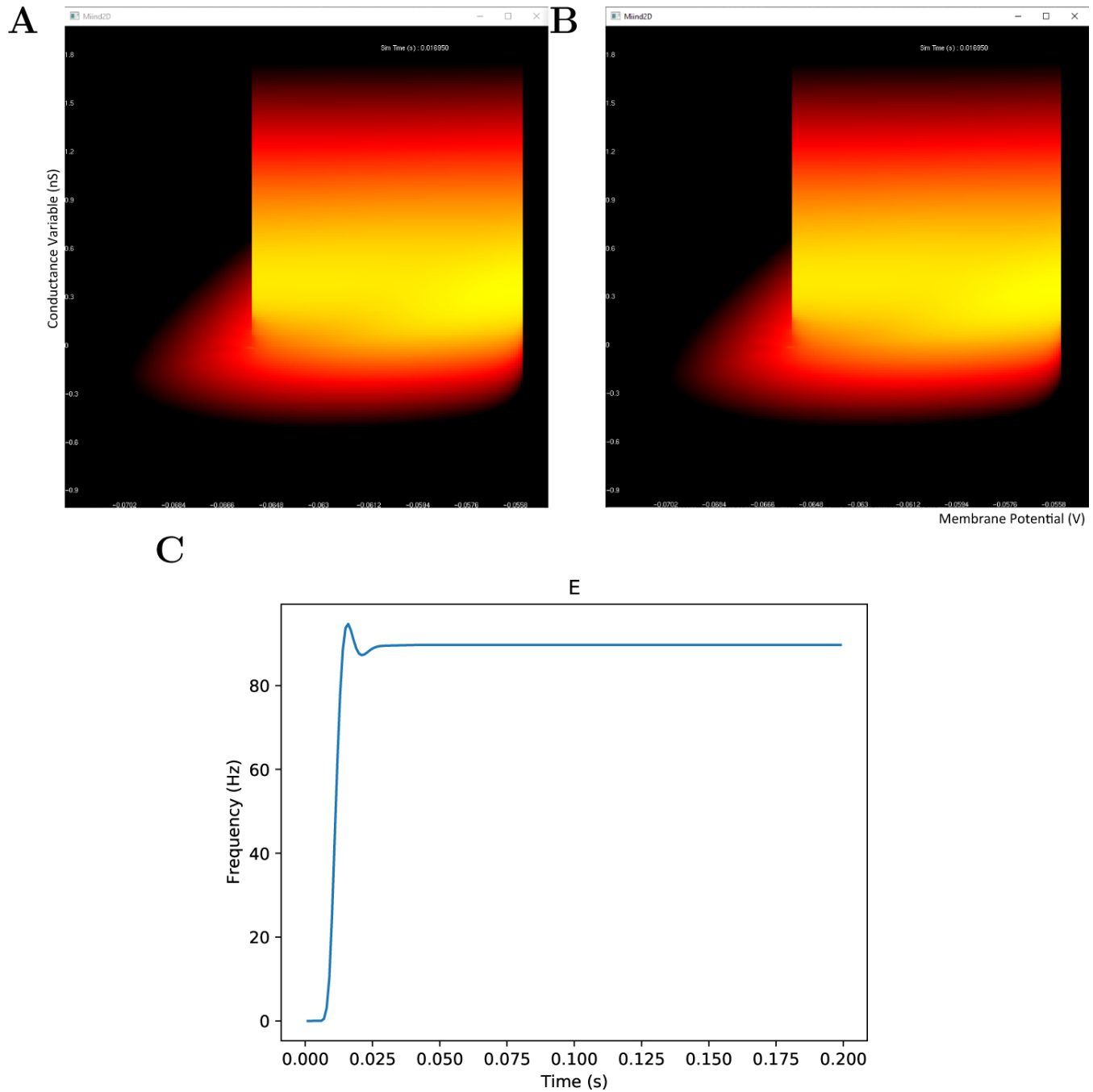


Figure 2. The display output of a running E-I population network simulation of conductance based neurons. (A) The probability density heat map of the excitatory population. (B) The probability density heat map of the inhibitory population. Brighter colours indicate a larger probability mass. The axes are unlabelled in the simulation windows as the software is agnostic to the underlying model. However, the membrane potential and conductance labels have been added for clarity. (C) The average firing rate of the excitatory population.

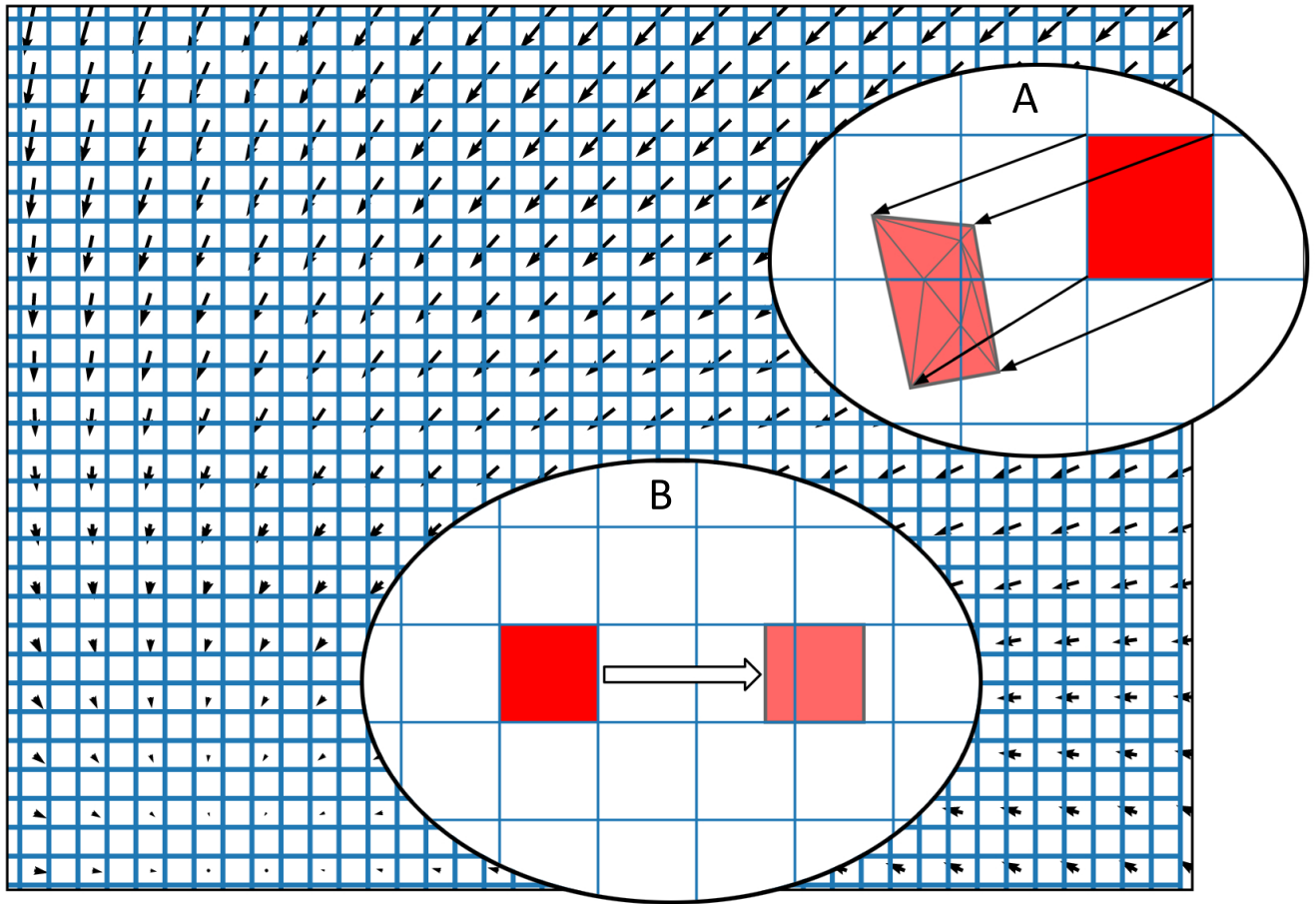


Figure 3. The state space of a neuron model (shown here as a vector field) is discretised into a regular grid of cells. (A) The transition matrix for solving the deterministic dynamics of the population is generated by applying a single time step of the underlying neuron model to each vertex of each cell in the grid and calculating the proportion by area to each overlapping cell. Once the vertices of a grid cell have been translated, the resulting polygon is recursively triangulated according to intersections with the original grid. Once complete, all triangles can be assigned to a cell and the area proportions can be summed. (B) For a single incoming spike (with constant efficacy), all cells are translated by the same amount and therefore have the same resulting transition which can be used to solve the Poisson master equation. In fact, the transition will always involve at most two target cells and the proportions can be calculated knowing only the grid cell width and the efficacy.

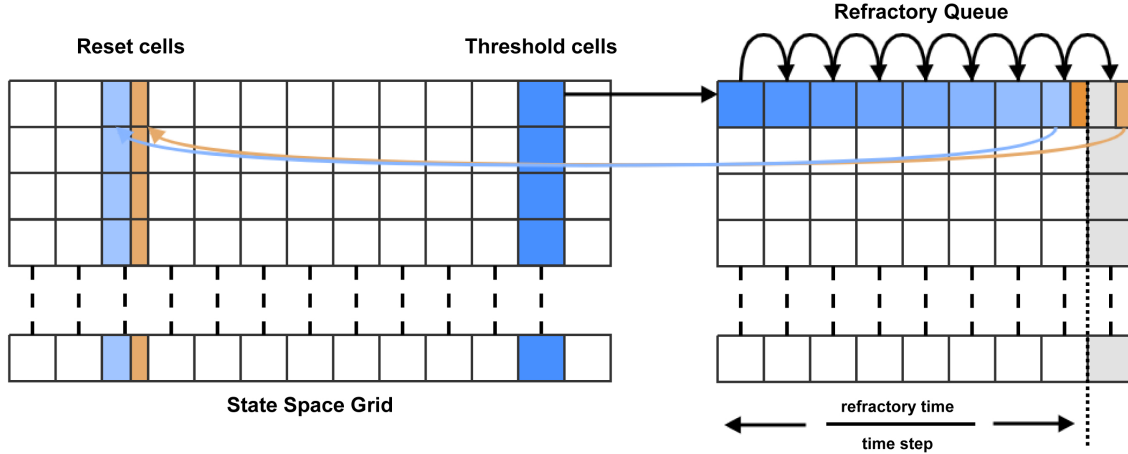


Figure 4. For each time step, probability mass in the cells which lie across the threshold (threshold cells) is pushed onto the beginning of the refractory queue. There is one queue per threshold cell. During each subsequent time step, the probability mass is shifted one place along the queue until it reaches the penultimate place. A proportion of the mass, calculated according to the modulo of the refractory time and the time step, is transferred to the appropriate reset cell. The remaining mass is shifted to the final place in the queue. During the next time step, that remaining mass is transferred to the reset cell.

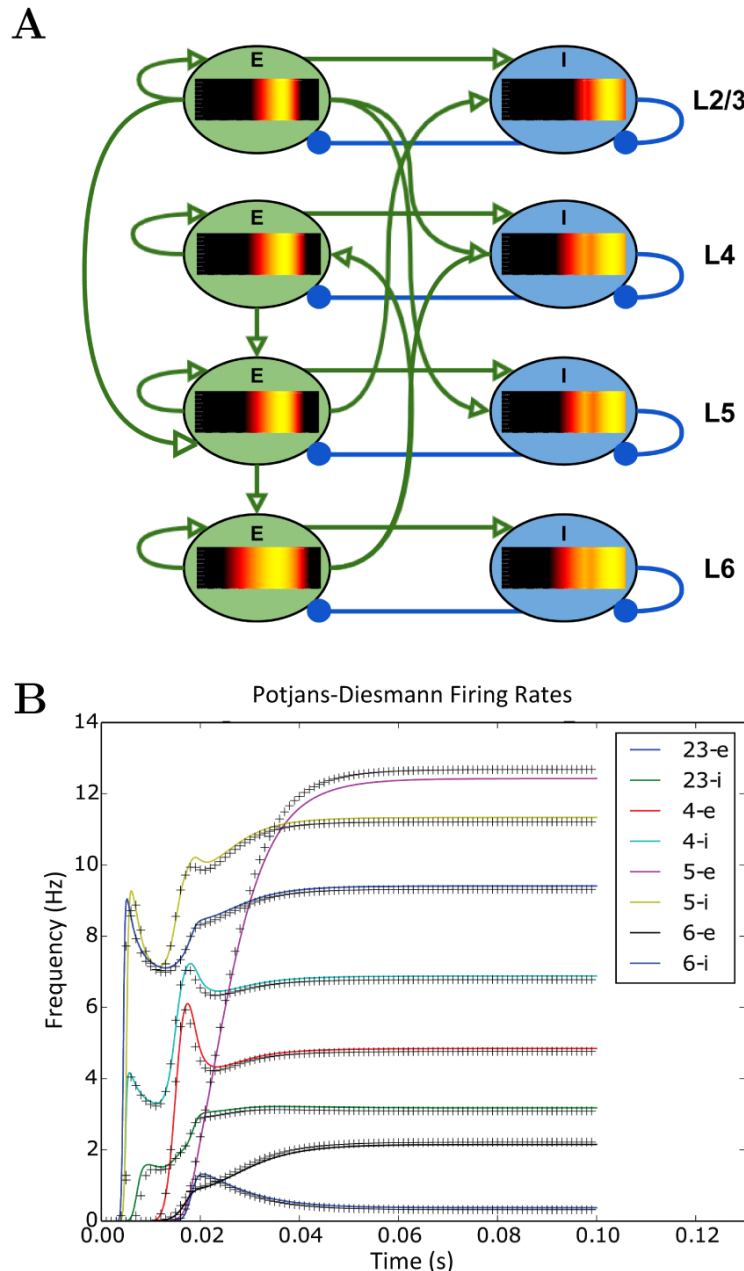


Figure 5. (A) A representation of the connectivity between populations in the Potjans-Diesmann microcircuit model. Each population shows the probability density at an early point in the simulation before all populations have reached a steady state. All populations are of leaky-integrate-and-fire neurons and so the density plots show membrane potential in the horizontal axis. The vertical axis has no meaning (probability mass values are the same at all points along the vertical). (B) The firing rate outputs from MIIND (crosses) in comparison to those from DiPDE for the same model (solid lines).

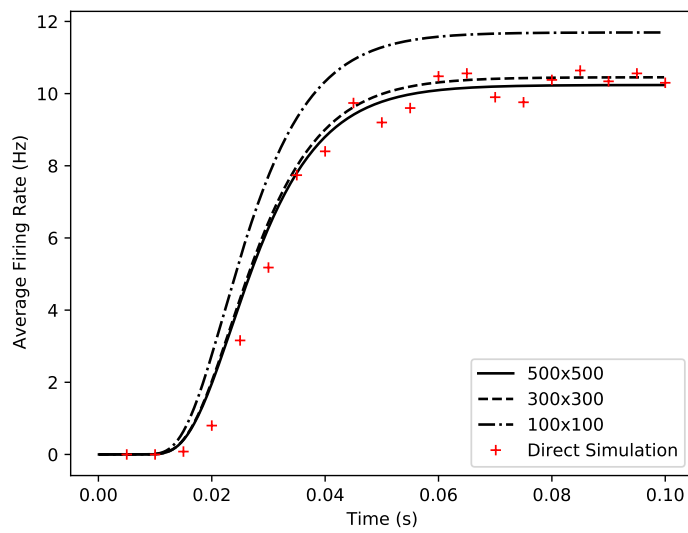


Figure 6. Comparison of average firing rates from four simulations of a single population of conductance based neurons. The black solid and dashed lines indicate MIIND simulations using the grid algorithm with different grid resolutions. The red crosses show the average firing rate of a direct simulation of 10,000 neurons.

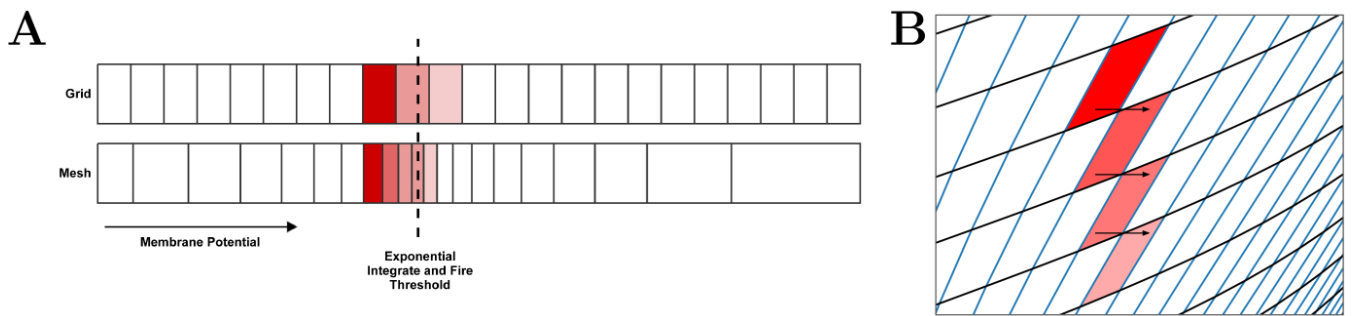


Figure 7. (A) In the grid algorithm, large cells cause probability mass to be distributed further than it should. This error is expressed most clearly in models where the the average firing rate of the population is highly dependent on the amount of probability mass passing through an area of slow dynamics. (B) In the mesh algorithm, when cells become shear, probability mass which is pushed to the right due to incoming spikes also moves laterally (downwards) because it is spread evenly across each cell.

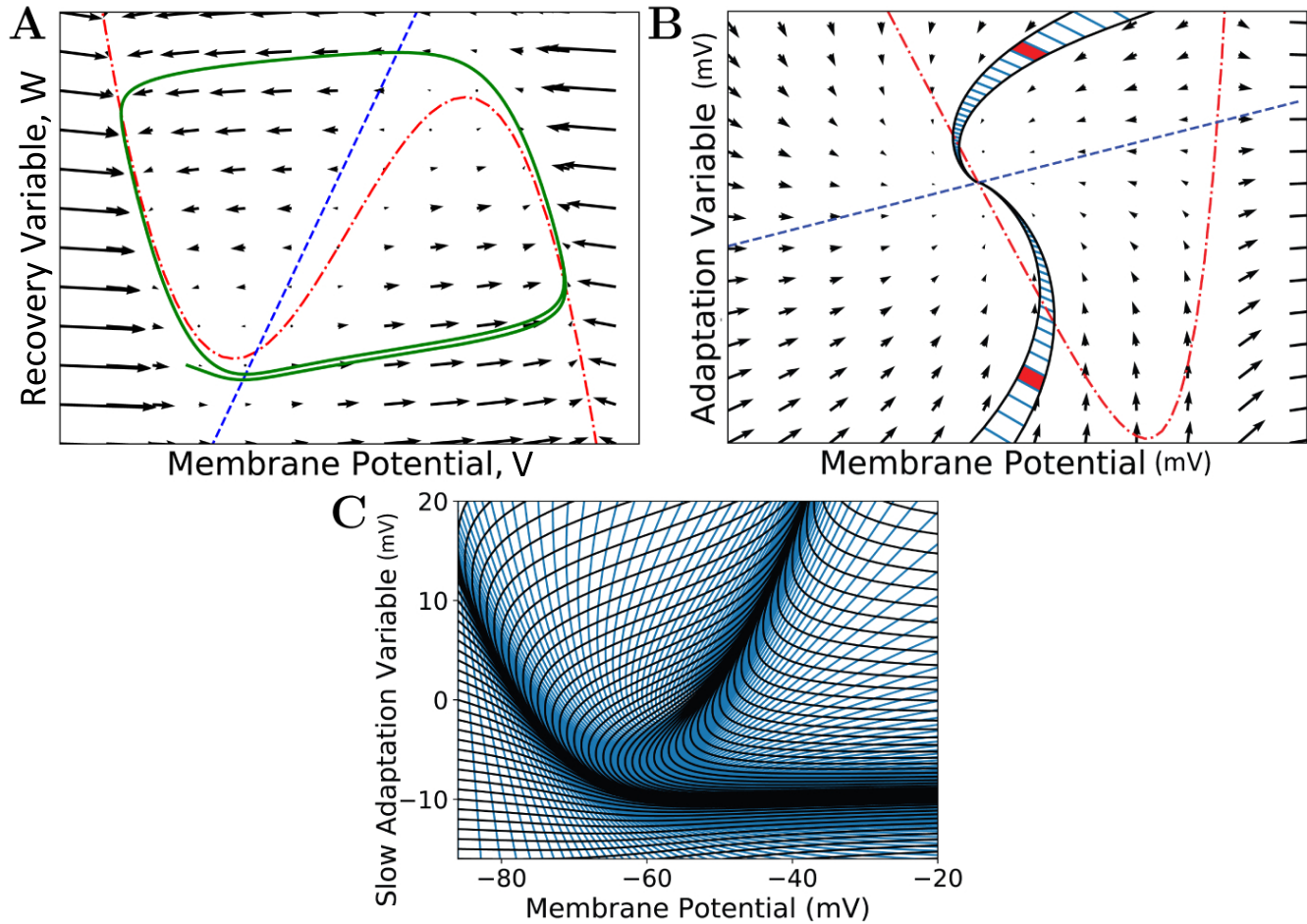


Figure 8. (A) A vector field of the FitzHugh-Nagumo neuron model (FitzHugh, 1961). Arrows show the direction of motion of states through the field according to the dynamics of the model. The red broken dashed nullcline indicates where the change in V is zero. The blue dashed nullcline indicates where the change in W is zero. The green solid line shows a potential path (trajectory) of a neuron in the state space. (B) A vector field for the adaptive exponential integrate and fire neuron model (Brette and Gerstner, 2005). Two strips are shown which follow the dynamics of the model and approach the stationary point where the nullclines cross. A strip is constructed between two trajectories in state space. Each time step of the two trajectories is used to segment the strip into cells. Because the strips approach a stationary point, they get thinner as the trajectories converge to the same point and cells get closer together as the distance in state space travelled reduces per time step (neurons slow down as they approach a stationary point). Per time step, probability mass is shifted from one cell to the next along the strip. (C) The state space of the Izhikevich simple neuron model (Izhikevich, 2003) which has been fully discretised into strips and cells.

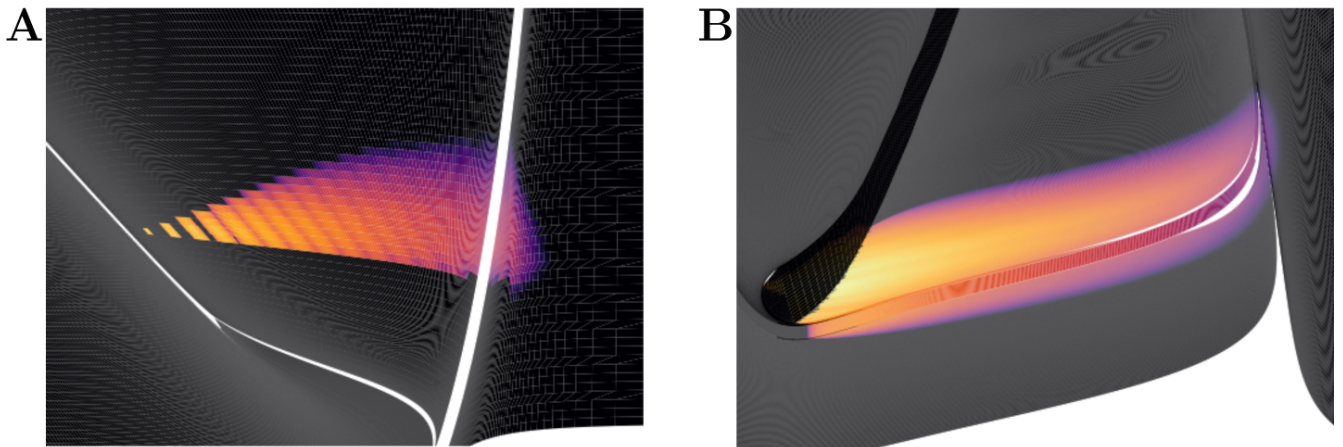


Figure 9. Heat plots for the probability density functions of two populations in MIIND. Brightness (more yellow) indicates a higher probability mass. (A) When the Poisson master equation is solved, probability mass is pushed to the right (higher membrane potential) in discrete steps. As time passes, the discrete steps are smoothed out due to the movement of mass according to the deterministic dynamics (following the strip). (B) A combination of mass travelling along strips and being spread across the state space by noisy input produces the behaviour of the population.

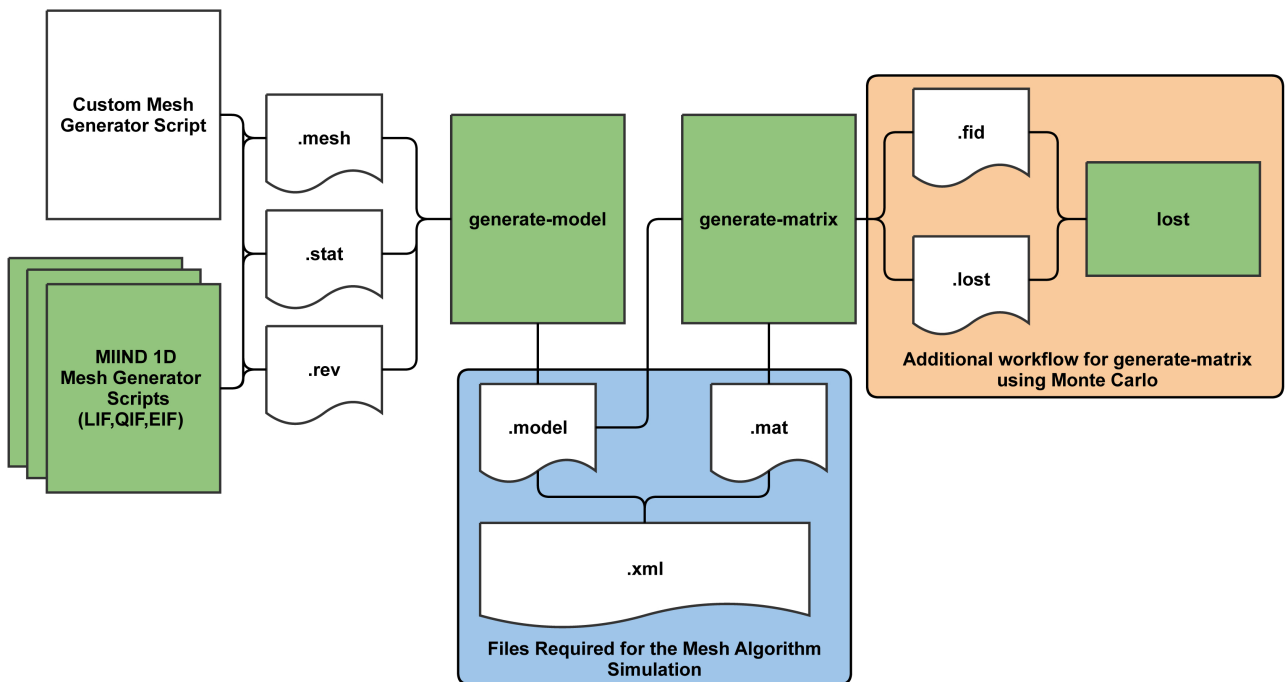


Figure 10. The MIIND processes and generated files required at each stage of pre-processing for the mesh algorithm. The shaded green rectangles represent automated processes run via the MIIND CLI.

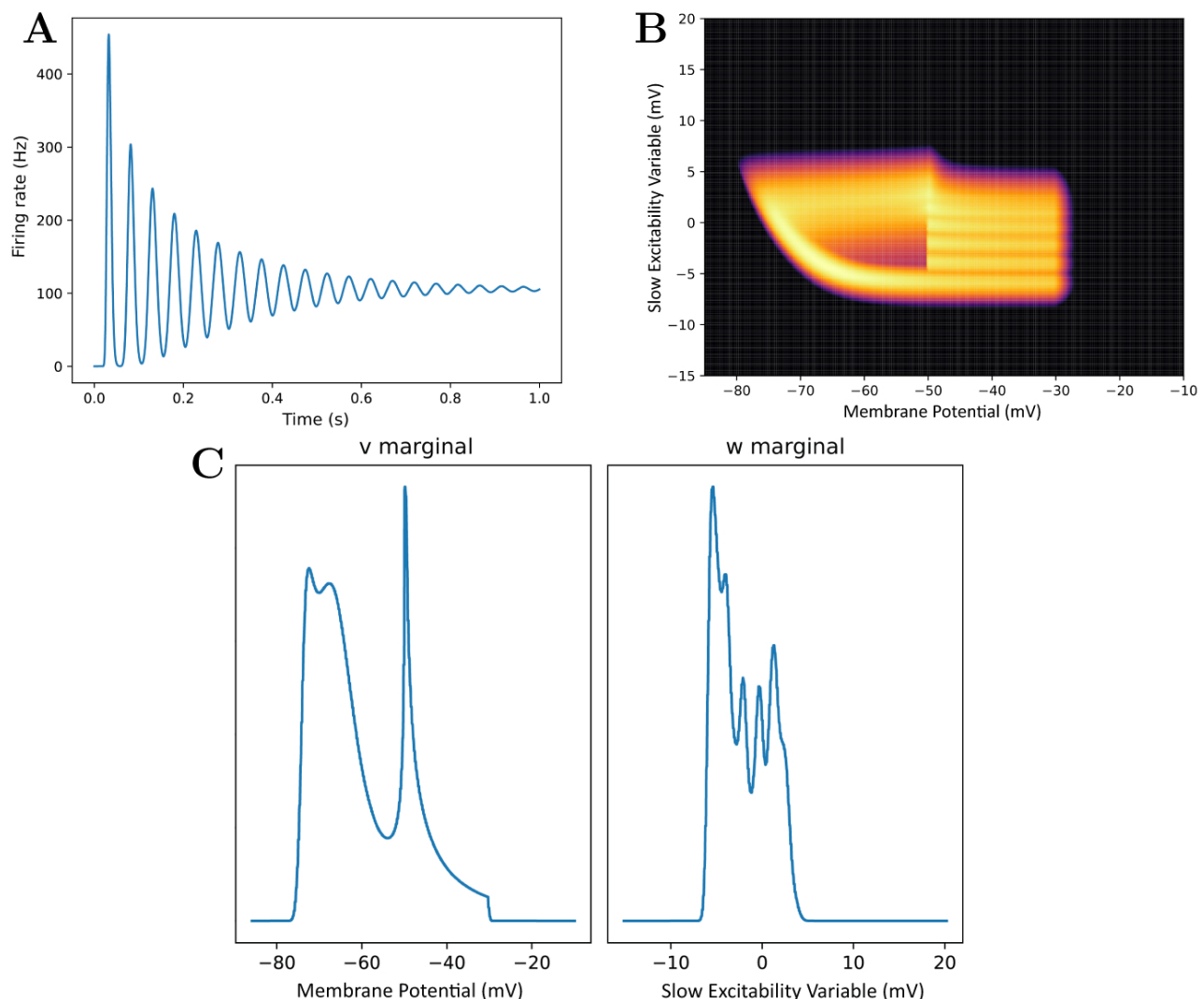


Figure 11. (A) The average firing rate of a population produced by calling the **rate** command. (B) A density plot of the population produced by calling the **plot-density** command. (C) The marginal density plots produced by calling the **plot-marginals** command.

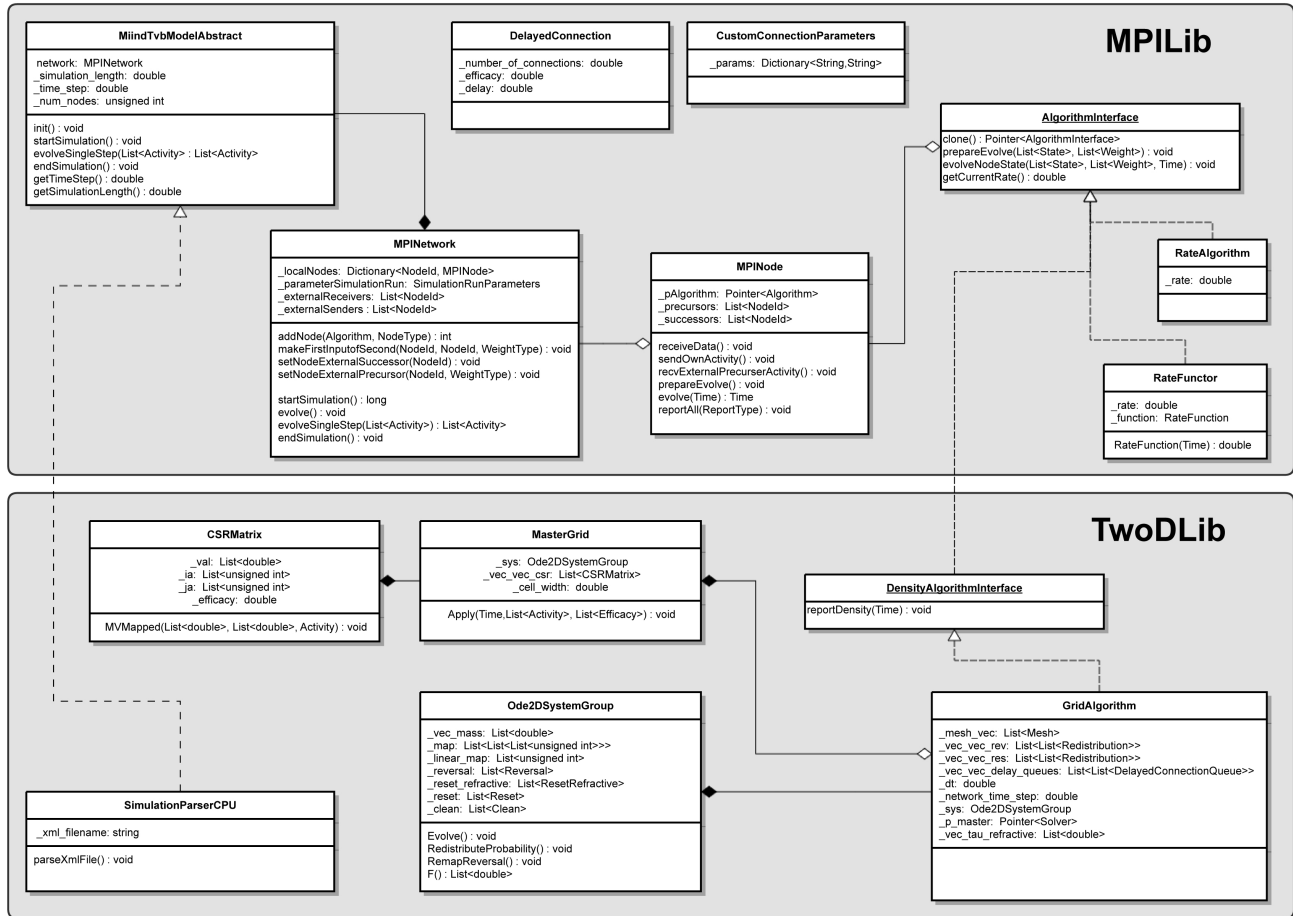


Figure 12. A minimal UML diagram of MIIND. The two major libraries, MPILib and TwoDLib, are represented.

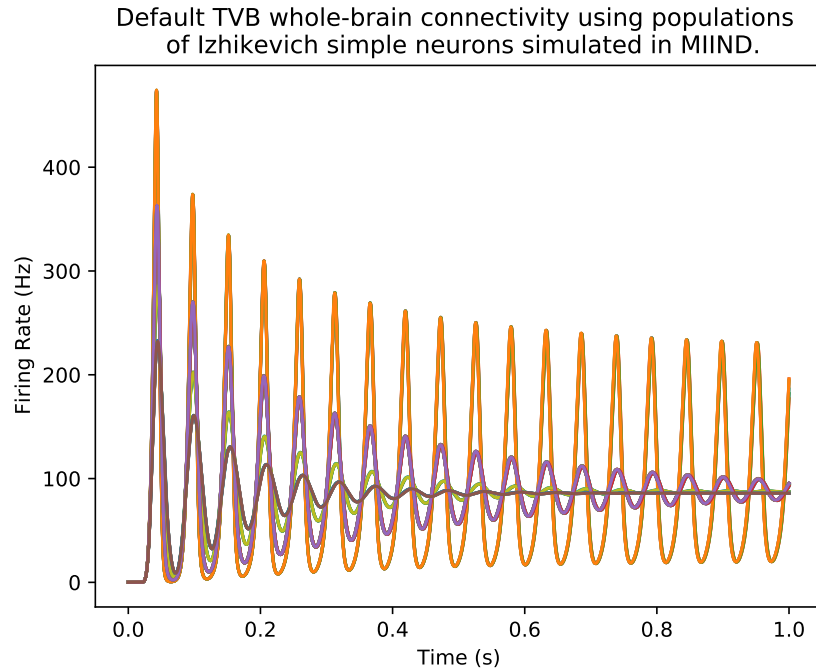


Figure 13. The firing rates of 76 nodes from the default TVB connectivity simulation. Each node is a population of Izhikevich simple neurons simulated using MIIND. The majority of nodes produce oscillations which decay to a constant average firing rate. However, a subset of nodes remain in an oscillating state.

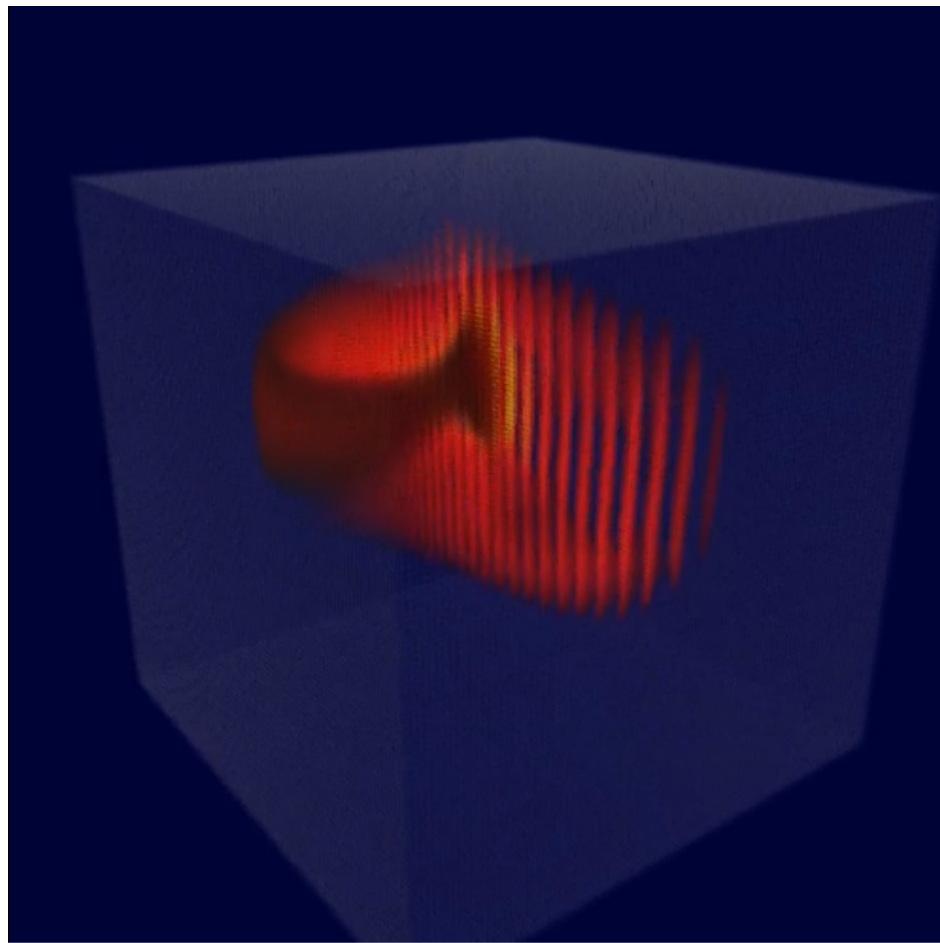


Figure 14. (A) A density plot of a population of Hindmarsh-Rose neurons. The density is contained in a three dimensional volume such that each axis represents one of the time-dependent variables of the model. The volume has been rendered from a rotated and elevated position to more easily visualise the density.